The Thesis Committee for Alexandra Lee Terpeluk
Certifies that this is the approved version of the following thesis:

Effects of Photocatalysis on Concrete Surfaces

APPROVED BY
SUPERVISING COMMITTEE:

Supervisor:

Maria Juenger

David Fowler

Effects of Photocatalysis on Concrete Surfaces

by

Alexandra Lee Terpeluk, B.S.C.E.

Thesis

Presented to the Faculty of the Graduate School of

The University of Texas at Austin

in Partial Fulfillment

of the Requirements

for the Degree of

Master of Science in Engineering

The University of Texas at Austin

May 2012

Dedication

I dedicate this thesis to the spirit of my uncle, Peter Terpeluk, Jr., who lived with true joy and enthusiasm.

Acknowledgements

I would like to thank my advisor, Maria Juenger, for her guidance during the writing of this thesis as well as for her invaluable insight and direction throughout entirety of the project. I would also like to thank my second reader, David Fowler, for his assistance in the completion of this thesis. Neil Crain and Clément Cros, it was a pleasure working with you and thanks for all of the hard work you did on your end.

I would like to especially thank Katy Aughenbaugh for training and assisting me with XRD, SEM preparation, and various other pieces of the puzzle. Thank you to Phil Pesek and Alex Garde for teaching me all about making concrete. Thanks to Chris Clement and Tony Bentivegna for consistently helping me to think of more efficient ways to get things done. Thank you to Eric Giannini for driving the truck when I needed to pick up the materials for the project. Thanks to Rachel Cano for all of her help with mixing concrete and the site visits.

I'd also like to express my gratitude to Mike Rung for his assistance with many parts of the project, including getting the field sites running and configuring the weather stations, and to Sherian Williams for her assistance in coordination of many details of the project. Thank you to Cliff Coward at TxDOT for his assistance with XRF. Thanks to Tom Juenger for loaning the spectrophotometer.

Thanks to everyone at CMRG who contributed to this project in some way and who broadened my knowledge and perspective. This project has been a tremendous learning experience and I'm grateful to all who have helped me along the way.

Abstract

Effects of Photocatalysis on Concrete Surfaces

Alexandra Lee Terpeluk, M.S.E.

The University of Texas at Austin, 2012

Supervisor: Maria Juenger

Highway air pollution is a significant environmental threat that has staggering implications for human health worldwide. Photocatalytic materials have the potential to reduce air pollution levels near major highways using ultraviolet radiation. This project, funded by the Texas Department of Transportation, evaluated photocatalytic efficiency and durability of several commercially-available photocatalytic coatings for use on concrete structures near highways.

The research presented in this thesis involved obtaining concrete highway barriers and creating concrete slabs for outdoor testing and laboratory chamber testing. Three commercially-available coatings were applied to the specimens for testing: Keim Soldalit® ME paint, TxActive® Stucco Cement, and Pureti Clean™.

Field sites were set up near major highways in Houston and Austin, Texas. Durability and photocatalytic efficiency were regularly monitored at the field sites using ion chromatography and spectrophotometry. X-ray diffraction (XRD) and scanning electron microscopy (SEM) were conducted on samples from each of the specimens

taken before and after placement at the field sites in order to understand durability of the photocatalytic materials that were exposed outdoors.

SEM results from this research project revealed that the photocatalytic material in the TxActive stucco and Keim paint remained in their original distribution after the exposure period, while the photocatalytic material in the Pureti Clean product appeared to decrease. XRD results remained fundamentally consistent for all coatings. Ion chromatography results showed that TxActive specimens had the highest surface levels of nitrates and nitrites between rainfall events, which indicates photocatalytic activity. Spectrophotometry results revealed a decrease in brightness for the Keim paint-coated specimens and no change or an increase in brightness for the TxActive stucco over time. The spectrophotometry results indicate how many surface contaminants are accumulating on the surface of a specimen, and thereby how efficiently sunlight is reaching the surface and activating the photocatalytic process.

Results obtained from this research project may be influential in the selection of a means for reducing highway pollution in Texas.

Table of Contents

List of Tables

List of Figures

Chapter 1: Introduction

1.1 Background

Air pollution is a growing environmental problem that has significant negative health implications for humans and other living organisms. According to the World Health Organization, 1.3 million people die each year worldwide due to causes related to urban outdoor air pollution (World Health Organization, 2011). Major primary pollutants that are produced by human activity include nitrogen oxides (NOx), which are emitted from combustion at high temperatures, and volatile organic compounds (VOCs), some of which play a role in the creation of ozone and are suspected carcinogens, among others. Since growing world populations imply that greater levels of pollutants will be generated through anthropogenic sources such as power plants and automobiles, significant efforts are being made to reduce air pollution levels and increase energy efficiency.

Photocatalytic materials are a promising technology that could help mitigate air pollution directly. When photocatalytic materials absorb ultraviolet radiation from the sun, hydroxyl radicals and superoxide anions are created that have the ability to react with pollutant molecules such as NOx to convert them to other, less harmful substances. This could be particularly advantageous in areas with high levels of air pollution, such as near major highways.

Several studies have found that the most efficient photocatalytic material for removing NOx and VOCs is titanium dioxide (TiO_2) in the anatase phase. Significant research has been conducted on TiO_2 incorporated into photocatalytic coatings for concrete specimens and incorporated directly into concrete, although few studies have been published that thoroughly test commercially available coatings in terms of photocatalytic activity. In addition, few tests have taken into account longevity of the

titanium dioxide-containing material, interaction of the photocatalytic material with the substrate, and durability of the material over long-term outdoor exposure. These are important considerations if this technology is to be successful in the long term.

1.2 RESEARCH OBJECTIVE

The objective of this research is to evaluate commercial photocatalytic coatings applied to portland cement concrete transportation structures to provide accurate data that are representative of highway applications. The research was intended to test coatings applied to concrete structures used in non-abrasive locations only. The best commercially available photocatalytic coating for highway infrastructure applications in Texas will be determined based on photocatalytic performance and material durability. Both laboratory testing and field testing are being conducted to accomplish these objectives. Field testing is being used to understand the effects of outdoor exposure on photocatalytic and material performance.

1.3 RESEARCH APPROACH

Concrete barriers were obtained from a local precast company for use in field testing. Concrete slabs (13.75 in. x 36 in. x 3 in.) were then prepared for both field and laboratory testing using the same materials, suppliers, and mixture proportions as the precast barriers. Four commercially available photocatalytic coatings were obtained for preliminary testing of photocatalytic efficiency and ease of application. Three of these products that showed the best performance were then selected for use in the field sites and additional laboratory testing. The selected coatings were applied to both types of concrete specimens, the slabs and the precast barriers.

Neil Crain and Clément Cros at the Center for Energy and Environmental Resources at The University of Texas at Austin conducted laboratory chamber testing for removal of pollutants by the coatings. An environmental chamber was assembled with the ability to analyze removal rates of ozone, nitrogen oxide and dioxide (NOx), and methane and non-methane hydrocarbons. In the first stage of this testing, the environmental chamber was characterized to determine that all equipment met manufacturers' specifications and to test the effect of the empty test chamber on the removal of pollutants. In the next stage, screening tests were conducted on the three coatings selected for preliminary testing. Finally, two coatings were selected and a full factorial experiment was run to test the effects of individual variables such as ultraviolet (UV) light intensity and relative humidity on photocatalytic pollutant removal. For each stage of the testing, an uncoated concrete specimen was also evaluated in order to determine whether plain concrete had any effect on pollution removal.

The three materials that were selected for preliminary chamber testing were also placed at each of the three field sites. Samples of each coated surface were removed from a barrier before placement at the field sites to analyze using scanning electron microscopy (SEM) and x-ray diffraction (XRD) to determine the spatial distribution and amount of TiO_2 material in the concrete substrate before outdoor exposure. Color was also measured using a spectrophotometer before exposure. Furthermore, the surfaces were washed with deionized water prior to placement in the field and the wash water was analyzed using ion chromatography for concentration of nitrates and nitrites, indicators of photocatalytic conversion of NOx.

Two field sites were selected at locations close to major highways in Houston and Austin, Texas. A third site was selected at J.J. Pickle Research Campus in Austin for

closer monitoring. Weather stations were set up at each of the sites to evaluate the impact of weather changes on photocatalytic activity and material performance. Barriers and slabs were placed at each of the sites and monitored every three months with water washes, spectrophotometry readings, and photographs. After a year of outdoor exposure, concrete slabs and barriers at each of the field sites were returned to the laboratory for further evaluation. Slabs were evaluated in laboratory chambers for photocatalytic performance. Samples were again taken from barriers and analyzed using SEM and XRD for the presence of photocatalytic material, changes in reaction products in the substrate, and durability of the material after one year of outdoor exposure.

1.4 SCOPE OF REPORT

Following this introductory chapter, Chapter 2 presents a literature review of the previous studies of photocatalytic materials for air pollution reduction that are relevant to the material evaluation component of the photocatalytic technology. The literature review is meant to include studies that pertain to the application method of photocatalytic material, properties of the photocatalytic material, interaction between substrate and photocatalytic material, and durability of photocatalytic specimens. This review covers studies that include photocatalytic material applied both as a surface covering and included in the concrete mixture.

Chapter 3 provides an overview of the experimental methods involved in the research. The procurement process and physical and chemical description for both the commercial photocatalytic coatings and concrete specimens are described. Mixture proportions and the mixing process for the concrete slab specimens are provided. Chapter 3 also includes a description of the methods used to characterize the specimens

before and after one year outdoor exposure, as well as the methods used to evaluate specimens in the field during the outdoor exposure period.

Chapter 4 provides results for the specimen characterization and field monitoring program. Differences in the distribution of TiO_2 before and after exposure are presented and discussed, as well as changes in color, composition of the water washes, temperature, and appearance. Weather station data in relation to these changes are also described and discussed.

Chapter 5 presents conclusions gained from this study and provides recommendations for future work related to evaluation of material properties and durability of commercial photocatalytic coatings applied to concrete highway structures.

Chapter 2: Literature Review

2.1 Titanium Dioxide Photocatalysts

Titanium dioxide (titania, TiO_2) is a naturally occurring compound that is used in a variety of applications, from consumer products to architectural coatings. It is also the preferred semiconducting material for photocatalytic applications (Husken et al. 2009). There exist in nature three main titanium dioxide structures, or phases: rutile, anatase, and brookite. Rutile is the most common and thermodynamically stable form and is used mostly as a paint pigment. Brookite is rare and has few general commercial applications (Beeldens & Van Gemert 2004). Anatase is chemically stable at room temperature, nontoxic, and economically favorable for use as a photocatalyst when compared to other semiconducting materials like ZnO (Husken et al. 2009). The most common, commercially available form of TiO_2 for photocatalysis is Degussa P-25, with an average primary particle size of 21 nm and an 80/20 anatase to rutile ratio (Strini et al. 2005). Many research projects investigating photocatalytic materials have utilized this commercial product for direct testing or for comparison to other semiconducting materials.

While anatase is generally considered the most practical and best-suited TiO_2 phase for photocatalytic applications, substantial research has gone into mixed-phase preparations. Toma et al. (2004) studied the removal of NOx gases by varying parameters of TiO_2 material including mass of catalyst, surface area containing the photocatalyst, and the anatase to rutile ratio, which was varied by changing the cooling temperature of heated P-25 powder. This study found that better photocatalytic removal occurred with higher ratios of anatase to rutile at temperatures below 600°C. Ozawa et al. (2005) claimed that mixed-phase titania preparations can have higher photocatalytic

performances than pure anatase or pure rutile in terms of reduction of acetaldehyde (CH_3CHO). They also stated that an anatase-brookite combination is more effective at reducing this same pollutant than pure anatase, probably due to the "anatase-brookite coupling, resulting in an increase in charge separation efficiency" (Ozawa et al. 2005).

Some researchers have explored creating photocatalytic materials through new processes or doped with metals to try to achieve improved photocatalytic efficiency. Znaidi et al. (2001) used a sol-gel method, in which hydrolysis and polymerization of a metal alkoxide are controlled at room temperature to produce an amorphous powder. By varying factors including pH, nature of alkoxide, hydrolysis ratio, and amount of dispersant, materials with slightly different particle sizes, surface areas, and densities of surface hydroxyl groups were produced. Znaidi et al. compared the photochemical activity of several different altered TiO_2 powders with commercial powders including Degussa P-25. Results of this research study showed that the commercial Degussa P-25 achieved higher photocatalytic degradation of phenol than the altered TiO_2 materials synthesized in the study.

Pepe et al. (2004) tested photocatalytic efficiency of TiO_2 materials doped with low amounts of metal ions. Both sol-gel prepared TiO_2 and commercial products were tested. The TiO_2 was applied to cementitious and marble substrates for testing. It was found that metal doping can result in enhanced photocatalytic degradation of pollutants, and that the magnitude of enhancement is a function of the nature of the doping elements, amount, and the structure of TiO_2. In particular, magnesium enhanced the photocatalytic activity of rutile; however, the magnesium-doped rutile material still had lower photocatalytic activity than the pure anatase form.

2.2 TiO_2 Application Methods

Many researchers have tested the efficiency of TiO_2 when added to cement during mixing of concrete, cement paste, or other cementitious materials. Dylla et al. (2010) tested the relative photocatalytic efficiency of four TiO_2-containing concrete mixtures by varying two material parameters, fines content and percentage of TiO_2. Concrete slabs were prepared with 3 and 5% by mass of cement weight of commercially available TiO_2 nanomaterial (Cristal Millenium PC105). The higher concentration of TiO_2 showed a slightly higher photocatalytic activity in this experiment; however, according to the authors, it was not certain whether this increase justified the higher cost associated with increased TiO_2 concentration.

Kawakami et al. (2007) studied NOx removal abilities, flow, and air content of three types of TiO_2 including solid forms of two different particle sizes and a colloidal suspension. Mortar specimens were prepared with TiO_2 as an additive to the cement. Ratios of TiO_2 to cement including 5, 10, and 15% were also tested for each of the three preparations. For the mortar specimens, they found that NOx removal decreased with increasing ratio of TiO_2 up to 15%, regardless of the TiO_2 preparation. The preparations with the smallest particle sizes of TiO_2 were found to be the best at removing NOx. The mortar specimens containing the finest particle size TiO_2 also exhibited considerably higher flow and lower air content compared to other preparations and regardless of ratio of TiO_2 to cement.

Several researchers studied the photocatalytic efficiency of TiO_2 applied as a surface covering. Hassan et al. (2010) conducted a study of several application methods of TiO_2 to the exterior of concrete pavement. The methods tested included a thin coating consisting of sand, cement, TiO_2, and water, a water-based hardened concrete surface

treatment commercially known as Pureti, and sprinkling nano-sized TiO_2 onto a fresh concrete surface directly after casting. Each method was evaluated in terms of photocatalytic efficiency. They found that the thin coating with 5% TiO_2 and the Pureti product were the most efficient at removing nitrogen oxide. Murata et al. (2000) found concrete paving blocks containing a 5-7 mm layer of TiO_2 in cement mortar to be an effective method for NOx removal.

Rachel et al. (2002) examined different application techniques of TiO_2-containing surface coatings including the sol-gel method, sputtering, and a patented method for coating inorganic fibers with TiO_2. Several sol-gel methods were used to produce the TiO_2 and then the material was applied by dip-coating. Sputtering refers to thin film deposition by ejecting atoms from a substrate through bombardment with energetic particles. An additional method in which TiO_2 was mixed with white cement and water to form a thin layer was also studied (Rachel et al. 2002). Each of these methods was compared in terms of photocatalytic efficiency. It was found that for certain substrates, the sol-gel method was less efficient than a TiO_2 slurry due to the comparatively smaller active surface produced by the sol-gel technique.

Agrios and Pichat (2005) compared the various preparations of TiO_2 onto fixed supports, including the sol-gel method and synthesis of mixed-phase TiO_2. Regarding films, they discussed several significant challenges of TiO_2 as a thin coating on organic materials, including thermal issues and photocatalytic degradation of the substrate. To counter this problem, sol-gel techniques can be performed at lower temperatures or through pressure, as in “cold sintering.” The use of an intermediate layer between the substrate and TiO_2 film can also reduce photocatalytic degradation issues (Agrios & Pichat 2005).

Two studies compared TiO_2 as an additive to cement to its application as a surface covering for mortar. Strini et al. (2005) found that a pure TiO_2 film achieves a much greater photocatalytic activity than samples with varying amounts of photocatalytic material added to the cement matrix. Diamenti et al. (2008) also compared TiO_2-containing mortars in which photocatalytic materials were added to the cement in powder form and as an aqueous suspension, and as a surface covering. This test found that the specimens containing TiO_2 as a surface covering were the most efficient.

Several studies examined commercial photocatalytic paints. Auvinen & Wirtanen (2008) tested six different interior photocatalytic paints with varying binder systems for their effects on indoor air quality in terms of elimination of VOCs. They found that an aged, water-borne lime paint achieved the lowest VOC removal, indicating that the chemical nature of the paints may change with aging. Varying the substrate, including glass, gypsum, or plaster, did not affect photocatalytic efficiency of the paints. Laufs et al. (2010) investigated the impact of pigmentation on reduction of NOx from commercial TiO_2-containing paints. They found that the non-photocatalytic TiO_2 contained in the white paint may have reduced the amount of active sites, thereby contributing to its decreased photocatalytic activity compared to a blue paint.

2.3 Substrate/TiO_2 Interactions and Durability of Photocatalytic Specimens

2.3.1 Effect of Substrate Properties on Photocatalysis

Many researchers explored the effects of the properties of the substrate onto which the photocatalytic substance was applied on photocatalytic efficiency. Fernandez et al. (1995) characterized TiO_2 applied to different rigid substrates including glass, quartz, and steel. Deposition on glass and quartz was conducted using a dip coating

procedure and on stainless steel by an electrophoretic deposition process. Samples were evaluated for photocatalytic activity and also for surface properties using x-ray photoelectron spectroscopy (XPS), scanning electron microscopy with energy dispersive spectroscopy (SEM/EDS), x-ray diffraction (XRD), and UV-VIS absorption spectroscopy. The quartz substrate specimen was found to show the greatest photocatalytic activity and also showed better crystallization of the anatase structure than the glass substrate. The TiO_2 deposited on steel had a greater percentage of rutile due to the high temperature associated with the deposition process. The migration of cationic impurities including Si^{4+}, Na^{+}, Cr^{3+}, and Fe^{3+} to the TiO_2 layers in glass and steel contributed to decreased photocatalytic activity of these prepared materials.

Rachel et al. (2002) studied the photocatalytic efficiency of Degussa P-25 TiO_2 applied to glass, cement, red brick, and inorganic fibers. These efficiencies were compared to that of Degussa P-25 in aqueous suspension. For the sputtering application, photocatalytic efficiency was negligible. For the sol-gel technique, it appeared that glass achieved higher photocatalytic efficiency than red brick or cement. The inorganic fibers achieved the highest photocatalytic activity of the materials tested, although the authors stated that method of application may have been more influential on photocatalytic efficiency than substrate composition. Auvinen & Wirtanen (2008), in their study of photocatalytic interior paints on indoor air quality, found that substrates had no noteworthy influence on photocatalytic behavior. The substrates tested included glass, gypsum plaster, and polymer-modified plaster.

Surface roughness of the substrate was found to be an important parameter governing photocatalytic efficiency. Husken et al. (2009) examined the application of two commercial TiO_2 products incorporated into concrete paving blocks. High surface

roughness was found to contribute to higher photocatalytic activity due to the availability of active surface area. Ramirez et al. (2010) found that higher surface roughness contributed to good adhesion of the photocatalytic material during the dip-coating process. For example, a plaster substrate retained most of the TiO_2 after dip-coating, which presumably is an indication of an ability to maintain photocatalytic activity. Weathering behaviors were also evaluated in this study, and it was determined that concrete substrates were less abraded than plasters. Surface roughness was shown to play a role in durability and adhesion of photocatalytic material in this case. Dehn et al. (2004) were in agreement with these results, recognizing the advantage of roughening the concrete surface so as to increase stability of a coating and thus, its reactivity.

Effect of Concrete Properties on Photocatalysis

Many studies addressed concrete substrates specifically, with photocatalytic material used as an admixture to cement or applied as a surface covering. Several researchers looked into designing a specific concrete mixture, using photocataylytic material as an admixture, that would enhance pollutant removal. Poon & Cheung (2007) discussed the influence of recycled materials incorporated into the concrete mix on photocatalytic efficiency. They found that recycled aggregate achieved a much higher removal than sand, and that this removal was enhanced slightly when furnace bottom ash was also incorporated. Higher porosity of the material was found to have a direct influence on photocatalytic activity. Incorporation of glass led to greater light transmittance of the concrete, allowing UV irradiation to penetrate the substrate more fully. Poon & Cheung (2007) also found that the recycled concrete with larger aggregate sizes achieved a higher porosity and therefore a higher photocatalytic activity. Ramirez et al. (2010) confirmed the relationship of porosity and photocatalytic efficiency in their

study, finding that TiO_2 adhered more successfully to porous substrates and thus achieved higher air purification. Ruot et al. (2009) measured pore size distribution directly and were able to show that higher porosity influenced photocatalytic efficiency. Dylla et al. (2010) studied the effect of varying both fines content and percentage of TiO_2 on photocatalytic efficiency. There was a significantly higher photodegradation rate achieved when fines were eliminated from the mix. Laufs et al. (2010), in their study on indoor paint, found that the addition of nonphotocatatlyic material into a photocatalytic paint reduced the photocatalytic activity by reducing number of pores and therefore active sites. Higher porosity mixes achieved higher photocatalytic activity, confirming the results found in the other studies.

Lackhoff et al. (2003) found that photocatalytic activity of several cementitious specimens with both TiO_2 and ZnO used as semiconductors was reduced due to cement ageing, most rapidly during the first four weeks. After eight weeks, it was found that photocatalytic efficiency stabilized. The authors suggested that this result could be explained by reduction of active sites due to carbonation. Carbonation decreases sorptivity, increases weight of cement, and can lead to calcite formation, which blocks the cement surface pores. Chen & Poon (2009) found that the number of active photocatalytic sites was the most important factor in determining photocatalytic efficiency. These authors found that NOx removal decreased with increasing curing age due to filling of capillary pores and carbonation.

2.3.2 Effect of TiO_2 on Substrate Properties

Several researchers looked at the effects of adding a photocatalyst admixture to concrete on the concrete property development. Both Jayapalan et al. (2010) and Lee et al. (2010) suggested that the addition of TiO_2 nanoparticles accelerates early hydration of

cement as additional nucleation sites are provided. Jayapalan et al. (2010) also suggested that nanoparticles increase the rate of concrete shrinkage. Lackhoff et al. (2003) found than concrete specimens containing TiO_2 photocatalysts had higher compressive strengths than those containing ZnO additions. Kawakami et al. (2007) found that compressive strength, modulus of elasticity and flexural strength decreased proportionally with increasing ratio of TiO_2 between 5% and 15%. These researchers also evaluated flow and air content of the mortars, and found these properties to be related to type of TiO_2 rather than its ratio to cement.

Zhang (2011) studied the impact of TiO_2 additions on the compressive strength of pavement concrete mixtures. Additions of 0.5, 1, 2, and 3% of TiO_2 by mass of cement were tested. Strength was enhanced with addition of nanoparticles most significantly for addition of 1% of TiO_2. Comparing the Zhang (2011) and Kawakami et al. (2007) studies, there appears to be an optimum amount of TiO_2, beyond which enhancement of strength properties is reduced. Zhang (2011) attributed this to a decreasing distance between nanoparticles, which disables calcium hydroxide from growing. When the ratio of calcium hydroxide to C-S-H gel is reduced, creep and shrinkage ensue and the cement microstructure loosens, reducing the strength of the concrete material. Murata et al. (2000) found that concrete paving blocks containing a layer of TiO_2 had comparable compressive strength and skid resistance to concrete blocks without a TiO_2 layer.

Zhang & Li (2011) looked at chloride permeability of two types of pavement concrete containing nanoparticles. Both SiO_2 and TiO_2 were tested. They found that TiO_2 was the more effective at reducing chloride penetration resistance. This is because the TiO_2 created finer concrete pore structures with higher resistance to chloride penetration.

2.3.3 Durability of Photocatalytic Specimens

Several studies examined the durability of photocatalytic specimens. Hassan et al. (2010) studied abrasion resistance and load wheel testing (LWT) for concrete specimens prepared with several types of photocatalytic coatings including Pureti, a thin coating similar to a stucco, and sprinkling TiO_2 on fresh concrete. Two concentrations of TiO_2 were used in the thin coating and sprinkling method, 3 and 5%. The highest NO removal efficiency after the load wheel test was found for the Pureti product. The highest removal after the rotary abrasion test was for the 5% thin coating. The results of the LWT indicate that NO removal efficiency of the weathered samples improved over the original state for all samples except the 5% TiO_2, which decreased only slightly in efficiency. The authors attributed this to the exposure of active sites below the surface caused by this type of weathering. Rotary abrasion appeared to decrease the NO removal efficiency for the 5% coating as well as the Pureti product, and improved it for the other specimens. All samples were evaluated using SEM and it was found that Pureti had a much more uniform distribution of TiO_2 compared to the sprinkling method.

Ramirez et al. (2010) also studied weathering resistance of photocatalytic materials on cementitious substrates. Cementitious specimens were prepared using the sol-gel method and then were exposed to varying abrasion conditions. Specimens were analyzed for retention of TiO_2 using SEM/EDS. The more porous and rough specimens were found to retain more TiO_2 particles after abrasion. For example, plasters were more affected by abrasion than concrete substrates.

Several researchers looked at durability of concrete using long-term outdoor exposure tests. Yu (2003) found that photocatalytic paving blocks became deactivated significantly after 4 months exposure in areas with high human intrusion levels. This was

attributed to the accumulation of non-polar species such as grease, since the blocks were placed close to restaurants and other areas of high human traffic. The conclusion of this study was that photocatalytic paving blocks should be placed in areas that do not experience high human intrusion. Motohashi & Inukai (2007) found that significant variation in soiling and durability between specimens occurred before and after five years outdoor exposure. By measuring wet methylene blue decomposition, it was determined that many coatings possessed significantly lower photocatalytic activity after the exposure. The authors recommended that future research address the specific causes for this reduction in efficiency so that the effect can be prevented if possible.

2.4 SELF-CLEANING PROPERTIES OF PHOTOCATALYTIC SPECIMENS

In many studies, self-cleaning properties of photocatalytic materials were considered. TiO_2 surfaces have the ability to maintain their cleanliness under ultraviolet light and can decompose organic matter that soils the surface (Fujishima et al. 2008). This self-cleaning behavior can be explained by the hydrophilic nature of TiO_2 surfaces, which results from the presence of hydroxyl groups at the surface of the material. These hydroxyl groups are increased with exposure to ultraviolet light. Water combines with these groups, causing sheeting instead of formation of water droplets at the surface of a TiO_2 coated material (Agrios & Pichat 2005). Sheeting of water aids in surface rinsing.

The hydrophilicity of photocatalytic materials can be measured through the contact angle of water applied at the sample surfaces. Diamenti et al. (2008) reported a decrease in contact angle of several samples after 4 days exposure to UV irradiation. They also found that the magnitude of decrease in contact angle was related to photocatalytic performance; the highest decreases were found with the most photoactive samples. Motohashi & Inukai (2007) evaluated the self-cleaning performance of several

commercial photocatalytic coatings over a five-year period of outdoor exposure. Even specimens that did not maintain significant photocatalytic activity after outdoor exposure did maintain low contact angles. Significant differences in both photocatalytic activity and contact angle were recorded for the range of commercial materials, which consisted of varying enamel paints containing TiO_2 or with TiO_2 painted as a top clear coat.

Self-cleaning properties were evaluated in a number of tests by measuring changes in color of the photocatalytic specimen. The CIE L*a*b* colorimetric system was used in many of these tests for evaluating changes in color. The CIE system is three-dimensional and is suitable for measurement of small variations in color over time. The a* value describes value between red and green, b* between blue and yellow, and L* between white and black. Motohashi & Inukai (2007), in the same study mentioned earlier, evaluated changes in L* values, which indicate brightness, using a color meter. All specimens evaluated in this study were white. Delta L* value results ranged from near zero to as low as -12, depending on the photocatalytic product that was used. These values were compared to degree of weathering for each of the coatings. Variations in these results occurred depending on the coating tested. The coatings that contained a polyurethane enamel paint, barrier primer, and TiO_2 clear coat had the best overall performance when considering both weathering and color changes.

Guerrini et al. (2007) conducted a colorimetric monitoring program for the "Dives in Misericordia" church in Rome, Italy, and the Music and Art City Hall in Chambery, France over six years of observation. The church in Rome, Italy saw little color changes with the exception of slight differences between internal and external sides of the large sails that make up the church's structure. Slight variations in the b* parameter may have been a result of the presence of inorganic substances that collected on the surface. The

Music and Art City Hall saw constant values of color, regardless of the directional position of the façade measured.

Chen et al. (2011) evaluated color changes of rhodamine B dye on various mortar mixtures with TiO_2 added to the cement matrix using the CIE L*a*b* system with a spectrometer. The dye faded at a rate that was independent of the content of TiO_2, indicating that the photocatalytic material was effective in discoloring the dye under UV irradiation through its self-cleaning ability. Diamanti et al. (2008) measured color changes of fiber-reinforced mortars with varying amounts of anatase in both powder and suspension forms. The samples, which were white at the beginning of the test, were monitored using a spectrophotometer for color changes. A change in color occurred for almost all samples that were exposed outside. A yellowing effect was exhibited by samples with higher photocatalytic activity.

Pepe et al. (2004) evaluated the self-cleaning properties of metal-doped TiO_2 specimens by recording time for photodegradation of an alcoholic extract of cigarette smoke on various photocatalytic specimens. In this study, nanosized TiO_2 contained in cement doped with magnesium or cerium achieved photodegradation of the substance in the least amount of time. Diffuse reflectance spectra were also recorded for the different materials.

Yu (2003) conducted a study of NOx removal efficiency of paving blocks in order to evaluate the possibility of deactivation of photocatalytic activity of blocks exposed to daily human intrusion. Washing was an ineffective means to regenerate photocatalytic activity, possibly due to the presence of non-polar species such as grease.

2.5 Field Tests of Photocatalytic Materials

Photocatalytic materials have been applied in many construction projects throughout the U.S. and the worldwide in recent years. Notable projects include the Basketball Facility at Louisiana State University, which architect Richard Meiers designed using TxActive photocatalytic cement to reduce effects of mildew in the wet environment of Louisiana. The I-35W Bridge reconstruction project in Minneapolis, Minnesota included the construction of 3 wavy 30' towers with TxActive photocatalytic cement incorporated into the mix. At Dalton State University, TxActive Aria was incorporated into the cement matrix in the construction of a tower to provide an iconic image for the school (Simms 2010). The photocatalytic materials in these projects were selected for their self-cleaning capacities and air quality was not monitored. In each case, self-cleaning goals have been successful based on visual inspections.

The Missouri Department of Transportation is currently undergoing improvements to Route 141, to be completed in Summer 2012. A portion of the highway will be constructed using a two-lift system in which the top lift utilizes photocatalytic cement concrete. Although no data have been recorded yet, pollutants in storm water runoff will be evaluated as part of the project to understand photocatalytic performance of the pavement. Temperatures of the section will also be monitored with numerous sensors. This project aims to minimize costs associated with inclusion of photocatalytic material while maintaining mechanical properties of the pavement (Stone 2010).

Chapter 3: Experimental Approach

The experimental approach for this project was determined in accordance with the research method described in Chapter 1. During the first part of the project, commercially available photocatalytic coatings were selected for testing and concrete specimens were obtained or cast. Outdoor exposure sites were then set up in three locations so that durability and changes in composition could be observed over one year under varying environmental conditions. Specimens were tested before and after exposure and monitored regularly throughout the exposure period. Meanwhile, each coated specimen was also tested in the laboratory chamber to calculate pollutant removal directly. This approach allowed for an understanding not only of photocatalytic performance, but also of each material's durability and interaction with its concrete substrate.

3.1 Exposure Site Monitoring

Three field sites were created to understand how the specimens would perform near major highways with significant air pollution from traffic. Two of the field sites were located near major highways in Houston and Austin, Texas, while the third was kept near the laboratory at the J.J. Pickle Research Campus in Austin.

3.1.1 Field Site Locations

The Houston site was selected as the Texas Department of Transportation district office located at 7600 Washington Avenue, close to I-10 in Houston, Texas. Figure 3.1 shows the location of the concrete specimens and weather station in relation to the highway. This field site is referred to throughout this thesis as the Houston field site.

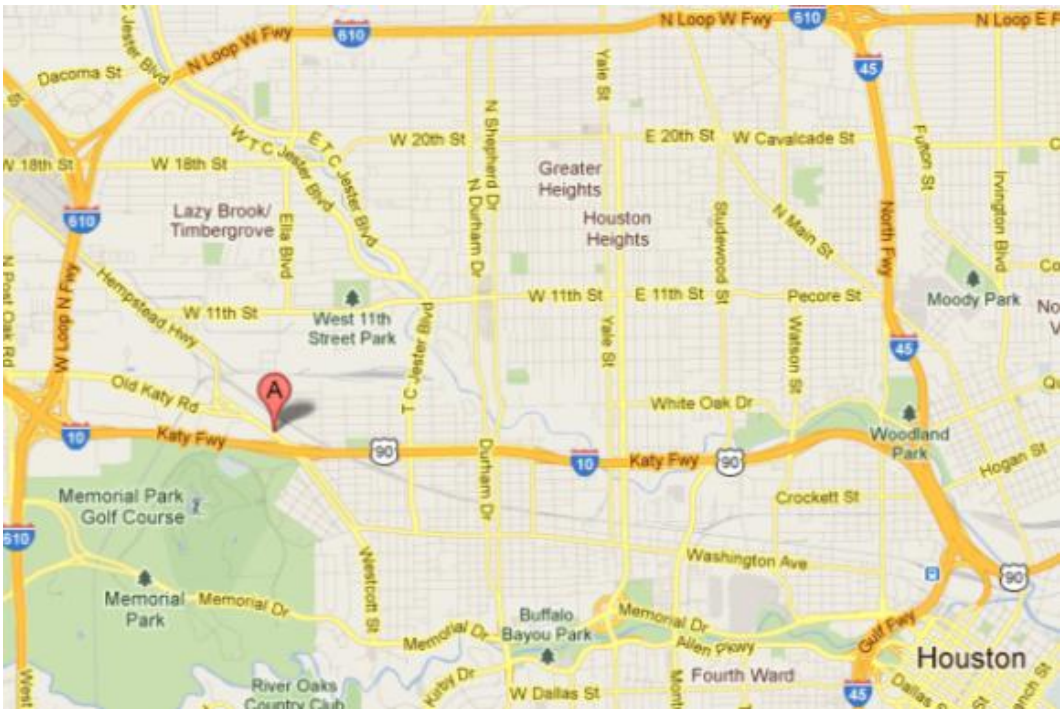

(a)

(b)

Figure 3.1: Houston Site (a) Aerial Map and (b) Facing I-10

The second field site was selected at the Texas Department of Transportation district office at 7901 North I-35 in Austin, Texas near the intersection of I-35 with Route 183. Figure 3.2 shows its location and proximity to I-35. This field site is referred to throughout this thesis as the Austin field site.

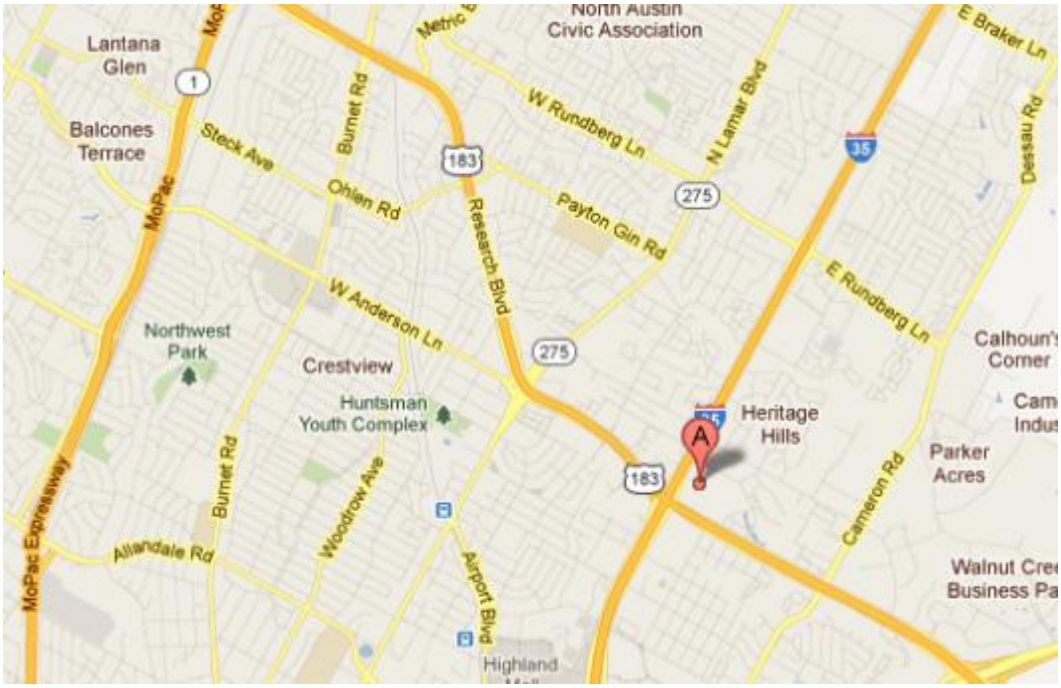

(a)

(b)

Figure 3.2: Austin Site (a) Aerial Map and (b) Facing I-35

The third location was at J.J. Pickle Research Campus at 10100 Burnet Road in Austin, Texas. This site was not directly adjacent to any major highway; however, its proximity to the laboratory allowed for more frequent monitoring and evaluation. Figure 3.3 shows its location. This field site is referred to throughout this thesis as the Lab field site.

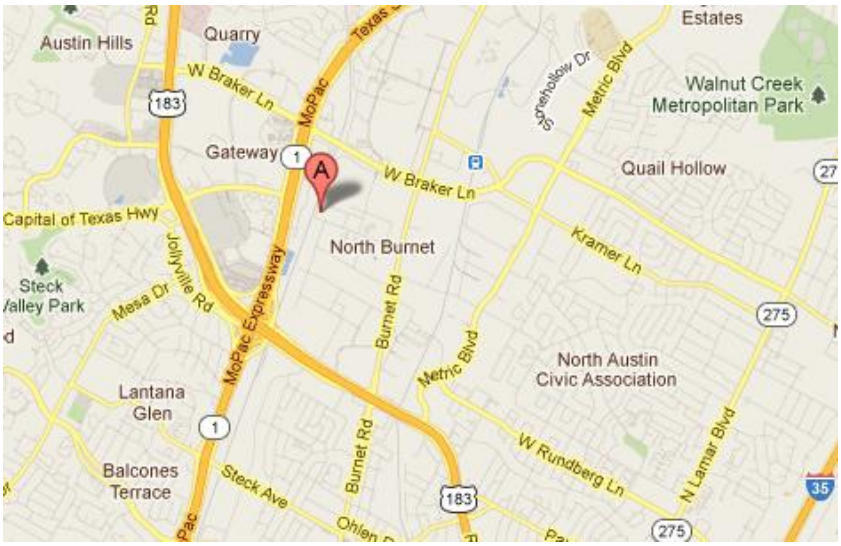

(a)

(b)

Figure 3.3: Lab Site (a) Aerial Map and (b) Facing North

3.2 MATERIALS PROCUREMENT

3.2.1 Procurement and Description of Commercial Photocatalytic Coatings

Several commercially available photocatalytic coatings were selected based on their commercial availability, performance in published testing, and relevance in terms of application procedure. Four products were selected for initial testing, with the intention that some would be eliminated from the project based on poor preliminary performance in the chamber tests or difficulty in application. The four products selected for initial testing included: TxActive® Stucco Cement, manufactured by Essroc; Soldalit®-ME paint, manufactured by KEIM; Pureti Clean™, manufactured by Pureti; and Photo-catalytic Spray, manufactured by Nirvana Safe Haven. The products were each applied to trial samples of concrete to determine ease of application. All products were applied to concrete substrates based on the manufacturer's recommendations.

TxActive® Stucco Cement is composed of portland cement, proprietary admixtures, and photocatalysts. The manufacturer recommends that when applying the stucco to concrete, surfaces be prepared in accordance with ASTM C926. For the final coat, the stucco is mixed with clean sand meeting ASTM C897 in a ratio of approximately one part TxActive® Stucco Cement to two to three parts sand by volume. According to the manufacturer's directions, two-thirds of the mixing water and one-half of the total sand volume are mixed and the stucco cement is then added to create the stucco. The remaining portion of the sand and sufficient water to achieve the desired workability are added. The stucco mortar is then mixed for at least 5 minutes until uniformity is achieved. Retempering (i.e. the addition of water) can be done once up until 1.5 h from initial mixing, at which time the stucco should be discarded. The stucco was applied to concrete using a hand trowel in a one-eighth-in. layer. To achieve a one-

eighth in. layer, approximately 500 g of stucco were used per full size slab, or 145 g/ft^2, or 1.56 kg/m^2. Figure 3.4 shows an example of the application method.

Figure 3.4: TxActive® Stucco Cement Application

The TxActive® Stucco Cement was analyzed using x-ray fluorescence (XRF)[1] and was found to contain approximately 5% TiO_2 by total mass. The stucco was also analyzed using x-ray diffraction (XRD) and found to contain anatase. The amount and type of TiO_2 for all coatings are shown in Table 3.1.

Table 3.1: TiO_2 Content of Commercial Coatings

Product Name	TiO_2 (% total weight)	Type of TiO_2
TxActive® Stucco Cement	5.0	Anatase
Keim Soldalit®-ME	9.7	Rutile
Pureti Clean™	1.0	Anatase
Nirvana Safe Haven Photo-Catalytic Spray	2.35	Anatase

[1] Clifton Coward at the Texas Department of Transportation Laboratory in Cedar Park, Texas performed all XRF testing reported in this study.

Keim Soldalit®-ME is a silica sol and water glass-based exterior paint that is appropriate for mineral substrates. According to the manufacturer's recommendations, the substrate must be dry, sound, non-chalking, clean and dust-free prior to application of the paint. Soldalit®-ME can be applied by paintbrush, roller, or airless sprayer and a minimum dry time of 12 hours is required between coats. The paint is applied in a two-coat process. The base coat is diluted with up to 5% KEIM Soldalit-Fixativ or up to 10% for strongly absorbent surfaces. The top coat consists of Soldalit-ME in its undiluted form. The two-coat system should be applied in a concentration of about 0.45 kg/m^2 for a smooth substrate, although exact values can only be determined during the application process. Figure 3.5 shows the paint application process.

Figure 3.5: Application of Keim Soldalit®-ME Paint

Undiluted Soldalit-ME paint was analyzed by XRF and determined to contain 9.70% TiO_2 by total mass, as shown in Table 3.1. The dried paint was also analyzed

using x-ray diffraction (XRD) and it was found that TiO_2 is present most prominently in the form of rutile.

Pureti Clean™ is a water-based photocatalytic spray that can be applied to virtually any surface, including both interior and exterior surfaces. Pureti Clean™ contains anatase TiO_2, titanium hydroxide, and de-ionized water. The product is applied by spraying to a clean surface only. A layer of Pureti's protective basecoat is first applied at a concentration of 0.2 kg/m^2. A layer of Pureti Clean™ is then applied in a concentration of 0.2 kg/m^2. The product can be applied using a sprayer or electrostatic spray system, although a sprayer was used for this application. Professionals from Pantheon Tile, a local distributor of Pureti products, applied this product to the concrete specimens at the Construction Materials Research Group (CMRG) building located at the JJ Pickle Research Facility. Figure 3.6 shows the application process at CMRG in April 2011.

Figure 3.6: Pureti Clean™ Application by Sprayer

According to the manufacturer, Pureti Clean™ contains 1% anatase by total weight, shown in Table 3.1. This product was not analyzed by XRF or XRD because it had an insufficient amount of solids for testing using these methods.

Nirvana Safe Haven Photo-Catalytic Spray is a water-based photocatalytic spray. According to the manufacturer, it should be applied 5 in. from a surface using a fine sprayer. It is applied in a concentration of 8 ounces per 250 to 500 square feet of surface. Figure 3.7 shows the application of Nirvana Safe Have Photo-Catalytic Spray.

Figure 3.7: Application of Nirvana Safe Haven Photo-Catalytic Spray

According to the manufacturer, Nirvana Safe Haven Photo-Catalytic Spray contains 2.35% anatase titanium dioxide by total weight, as shown in Table 3.1. Nirvana Safe Haven Photo-Catalytic Spray was eliminated from testing prior to the installation of the field sites due to poor results in preliminary chamber testing.

Two additional coatings were procured at the end of the project for additional air chamber testing. Stucco that did not contain photocatalytic material was tested to better understand pollution removal qualities of the TxActive stucco. The second coating was a

photocatalytic slurry, manufactured by TxActive, that did not become available until the end of the project. One full size concrete slab was coated with each of these products; however, they were not used in any testing other than the environmental chamber testing conducted by Clément Cros and Neil Crain.

3.2.2 Procurement and Description of Concrete Specimens

Two types of concrete specimens were selected for testing, barriers and slabs. In order to accurately understand the performance of concrete transportation structures with photocatalytic coatings, actual sections of highway barrier were obtained from Tricon Precast Ltd., located in New Braunfels, Texas. Three 5-foot sections of barrier were purchased, one for each of the three field sites. Each barrier was divided into four sections of equal width. To divide the sections, strips of aluminum flashing were installed using both mechanical anchors and flashing sealant. Sections were prepared and coated according to the manufacturers' recommendations, one each for TxActive® Stucco Cement, Keim Soldalit® ME paint, and Pureti Clean™. The fourth section of each barrier was left uncoated for monitoring as a control section. A drawing with details of the dimensions and sectioning for the highway barrier specimens is shown in Figure 3.8.

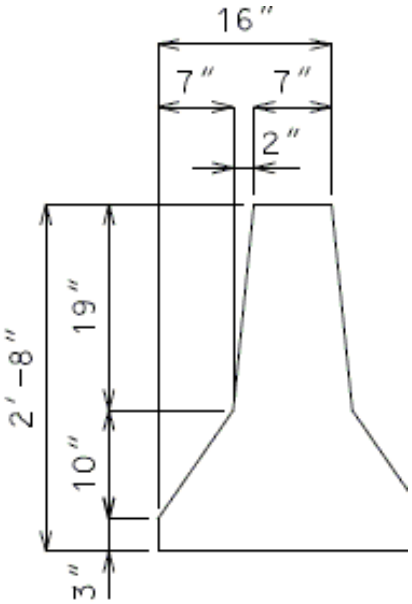

(a)

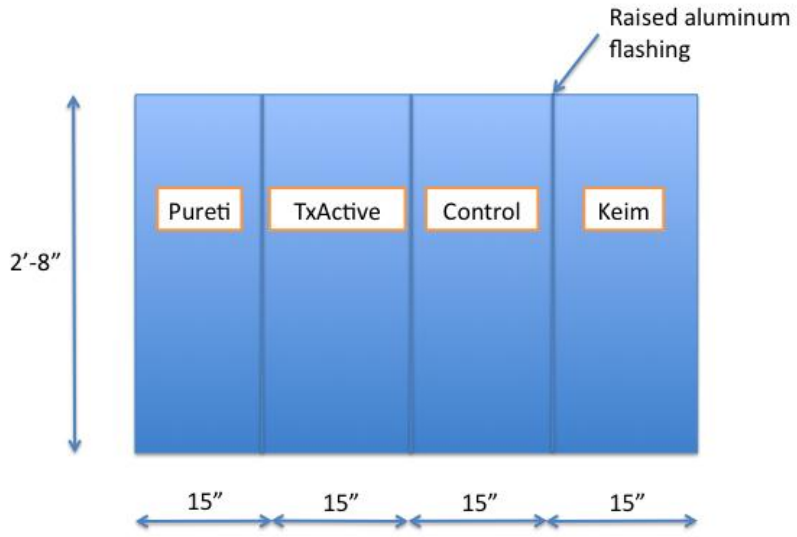

(b)

Figure 3.8: Concrete Barrier Specimen (a) Side Elevation (b) Front Elevation

In addition to the barrier specimens, full size concrete slabs were created for both chamber testing and field testing. The dimensions of the full size slabs were determined based on the size of the chamber. In addition to the full size slabs, half size slabs were also created for chamber testing towards the end of the project. These half size slabs were not placed at any field sites and were only used in chamber testing. Figure 3.9 shows the dimensions of the full and half size slabs.

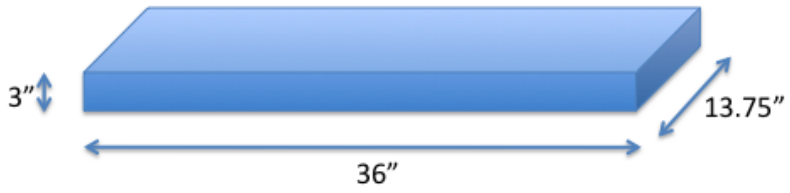

(a)

(b)

Figure 3.9: Dimensions of (a) Full Size and (b) Half Size Slab Specimens

Formwork was prepared using wooden boards, plywood, screws, and L-shaped brackets for securing. Adhesive-ready Teflon® PTFE sheets were obtained, cut to size, and placed on the bottom face of the formwork. The purpose of the Teflon was to create

a smooth surface for coating without applying any greases or oils that could interfere with the air chamber testing. An example of completed formwork is shown in Figure 3.10.

Figure 3.10: Completed Slab Formwork

The slab specimens were created for both testing in the environmental chamber as well as for placement in the field sites. One slab was prepared and coated for each of the three commercial coatings to be tested, and a fourth slab was prepared and left uncoated

for use as a control specimen. A set of four slabs was placed at each of the three field sites. The purpose of placing slabs at each of the field sites was to allow for chamber testing after one year of outdoor exposure. In total, each field site contained four slabs and one barrier section, with each barrier divided into four subsections. Four slabs were also made and left uncoated for placement outdoors. After one year of exposure, these slabs were coated and tested in the environmental chamber to determine the effect of the exposure period on photocatalytic performance. Table 3.2 shows the locations and coatings of all concrete specimens involved in this project.

Table 3.2: Type and Location of Concrete Specimens

Exposure site location	No. slabs	Description of slab coatings	No. barriers with 4 subsections	Description of barrier subsection coatings
Houston	4 Full size	1 TxActive stucco 1 Pureti 1 Keim 1 control (uncoated)	1	1 TxActive 1 Pureti 1 Keim 1 control (uncoated)
Austin	4 Full size	1 TxActive stucco 1 Pureti 1 Keim 1 control (uncoated)	1	1 TxActive 1 Pureti 1 Keim 1 control (uncoated)
Lab	8 Full size	1 TxActive stucco 1 Pureti 1 Keim 1 control (uncoated) 4 uncoated for later coating and testing	1	1 TxActive 1 Pureti 1 Keim 1 control (uncoated)
Environ. Chamber	6 Full size 4 Half size	1 TxActive stucco full size 1 Pureti full size 1 Keim full size 1 control (uncoated) full size 1 non-photocatalytic stucco full size 1 TxActive slurry full size 1 TxActive stucco half size 1 Pureti half size 1 Keim half size 1 control (uncoated) half size	0	N/A

3.3 CONCRETE SLAB SPECIMEN PREPARATION

3.3.1 Materials

The materials used for mixing the concrete slab specimens were selected based on typical materials and materials suppliers used by Tricon Precast in their mixture design for highway barriers. The cement selected was an ASTM C150 Type III cement from Capitol Aggregates in San Antonio, Texas. The supplementary cementitious material was a Headwaters Limestone Class F Fly Ash from Jewett, Texas complying with ASTM C618.

The coarse and fine aggregates were obtained from the Hanson Servtex plant in New Braunfels, Texas. Both aggregates were composed of limestone. No additional sieving or re-proportioning was done after receiving the aggregates. The coarse aggregate had a maximum aggregate size of 1 in., which was chosen based on both practicality in regard to proposed slab thickness and actual size used by Tricon Precast in the production of highway barriers. The absorption and specific gravity of the coarse and fine aggregates were calculated according to ASTM C127 and ASTM C128, respectively, and are listed in Table 3.3.

Table 3.3: Absorption and Specific Gravity of Aggregates

Aggregate Type	Absorption (%)	Specific Gravity
Limestone Coarse	1.86	2.59
Limestone Fine	1.84	2.61

3.3.2 Mixture Design

The mixture design for the slab specimens was determined based on the typical mixture design used by Tricon Precast in the preparation of highway barriers. Therefore, the concrete mixture design was kept consistent between the two types of specimens that were used in this project. The concrete mixture was a 25% fly ash replacement of Type III cement with a nearly 1:1 ratio of coarse to fine aggregate. The mixture design obtained from Tricon Precast is shown in Appendix A. Also provided in Appendix A is the mixture design used in creation of the slab specimens, which was taken from the Tricon Precast design and adapted for the volume of concrete necessary for the slabs, cylinders, and fresh property tests.

3.3.3 Slab Specimen Batching, Mixing, and Testing Procedures

This section describes the procedures for preparing the concrete slab specimens. The processes for batching, mixing, and testing of the hardened concrete are described. The procedures followed for batching and mixing of concrete were in accordance with ASTM C192: Standard Practice for Making and Curing Concrete in the Laboratory, with specific guidelines from Pesek (2011).

3.3.3.1 Batching

All of the aggregate and cement for the concrete mix was batched at least 24 hours prior to mixing. Approximations of correct weights of coarse and fine aggregates were obtained from outdoor storage bins. The coarse aggregate was placed in the concrete mixer first and a small amount of water was added. The aggregate and water were combined in the mixer for 1-2 minutes to allow the aggregate to achieve saturated surface dry (SSD) condition. The aggregate was then placed into 5-gallon buckets and weighed. A small amount of aggregate was removed and placed in a small container to

determine moisture content (Pesek, 2011). The process was repeated for the fine aggregate. Finally, the correct weights of cement and fly ash were gathered and placed in buckets to store inside the temperature-controlled mixing room.

3.3.3.2 Mixing Process

Just prior to mixing, the samples of aggregate that were removed for determining moisture content were weighed once again and the moisture content for both fine and coarse aggregate was determined. Based on these calculations, corrections were made to the weights of coarse and fine aggregate as well as the weight of water. Chemical admixtures and water were each weighed out separately and then mixed together. The concrete mixer, wheelbarrow, and materials to be used for quality control testing were each wetted slightly with water.

Next, the fine and coarse aggregates were placed in the concrete mixer with approximately one-third of the mixing water. The aggregate and water mixture was mixed for approximately 1 minute. At this point the mixer was stopped and the cement and fly ash were added. After placing a lid on the mixer opening, the mixer was started again and allowed to run for about 30 seconds. Figure 3.11 shows this concrete mixing procedure step.

Figure 3.11: Concrete Mixing Procedure

Then the lid was removed, and the remaining two-thirds of the water was added in a slow, steady stream while the mixer was rotating. The mixer was then run for approximately 3 minutes, stopping only to break up any material that appeared to adhere in large, unmixed clumps as necessary. Once the 3 minutes were complete, the mixer was stopped and the mixture was allowed to rest for a total of 3 minutes. At the conclusion of this three minute resting period, the mixer was started again and the mixture was mixed for an additional 2 minutes. At the end of this period of time, the concrete was placed into a wheelbarrow and moved to a location where it could be placed easily by shovel into the prepared slab formwork. The concrete was placed into the forms and then vibrated for approximately 3 minutes to ensure an even distribution of aggregate and relatively smooth top surface. The quality control tests, described in the following section, were also performed at this time.

3.3.3.3 Concrete Quality Control Testing

Fresh concrete was tested in terms of slump, unit weight, and air content for each mix. These tests were performed in accordance with the following ASTM standards:

- Slump: ASTM C143 (2010)
- Unit Weight: ASTM C138 (2010)
- Air content: ASTM C231 (2010)

In addition, three 4-in. x 8-in. cylinders were cast per mix for 28-day compressive strength testing of hardened concrete. For mixtures 1 through 9, hardened cylinders were cured by the same procedures as for the concrete slab specimens. For mixtures 10-14, the cylinders were cured according to ASTM C 39 (2010). To account for the lower number of mixtures cured according to the ASTM standard, 6 cylinders were cast for these mixtures. This allowed actual strength of the slab specimens to be measured under the specific curing conditions. The results for the different types of curing conditions could then be compared.

3.3.4 Slab Specimen Curing and Coating Procedures

All concrete slab specimens were cast in wood forms and demolded after 24 hours. They were then kept in a 73°F, 100% relative humidity chamber for 6 days to represent ideal curing times. After 6 days, the specimens were moved to a laboratory room with a 73°F, 50% relative humidity environment for 14 days to equilibrate to a lower moisture rate. By keeping the curing times and conditions consistent, these factors could be eliminated as variables in the testing. All specimens were coated after 21 days ± 24 hours. The formwork-finished side of each specimen was used for coating to most accurately represent surfaces of actual highway structures. The manufacturers' recommended procedures were followed for coating the specimens, as described in

Section 3.1.1. In order to isolate the flat surface of each sample as a variable in the chamber testing, the sides and bottom of each slab were coated with sodium silicate. This sodium silicate coating prevented the sides and bottom of each slab from having any effect on lowering pollution during the chamber tests.

3.4 Specimen Characterization Before and After Exposure

All specimens to be placed in the field sites were characterized before and after one-year exposure. The field site specimens were characterized using x-ray diffraction (XRD) and scanning electron microscopy (SEM).

3.4.1 X-Ray Diffraction

Small cores (3-in. diameter, ½-in. depth) of concrete were removed from the coated sections of the Lab barrier prior to one-year outdoor exposure. Two cores were removed from each of the coated subsections of the barrier, one for SEM and one for XRD. The sections were removed at the surface of the barrier using either a Hilti TE-C-BK-TW percussion core bit or a Hilti DD 120 coring rig. Samples were assumed to be approximately similar between the barriers and slabs with a given coating before exposure, and therefore sections were only taken from one barrier in the initial state. Cores were then taken from all of the barriers and slabs after one year of exposure.

The samples to be used for XRD were crushed using a Scienceware Micromill grinder until they passed through a #325 sieve (45 μm). The samples were then placed in vials and stored under vacuum until they were tested. When ready for testing, the samples were loaded into the holders and placed in the Siemens D500 diffractometer. Samples were scanned from 10°-70° 2θ. Samples were analyzed for the presence of different forms of TiO_2 as well as for concrete reaction products. The presence of TiO_2

and reaction products were compared for specimens before and after exposure to better understand the effect of outdoor exposure on composition of a concrete specimen coated with photocatalytic material.

3.4.2 Scanning Electron Microscopy

The second core of concrete that was obtained from the specimens was used for SEM. It was first broken in half using a hammer and chisel to create two sections. The first section was reserved for viewing the fractured surface using SEM. The second section of concrete was sliced to approximately 0.24 in. (6mm) thickness with a Buehler Isomet 1000 precision saw using ethanol as the lubricant. This piece was used to view a cross-section of the concrete and coating. The sawed sample was placed under vacuum for at least 24 hours prior to epoxy impregnation. The procedure followed for epoxy impregnation was from Williams (2006). The grinding and polishing times were following Drimalas (2007). The cross section samples were placed in a two-part epoxy resin from Epoxy Technology using an epoxy impregnation device so that a vacuum could be held on the samples during placement. The samples were allowed to cure for 24 hours at 73° F prior to removal from the holder.

After fully curing, the samples were removed from the holders and ground with #180, 400, 800, and 1200 grit sandpaper by hand. The samples were moved to finer grit sandpaper when scratches on the specimen and the stabilization of the width of cracks within the sample revealed that grinding at a particular level was complete. Typically, this took approximately 10-15 minutes per grit size. After grinding, the samples were polished with 3, 1, and ¼ micrometer diamond paste. The samples were polished using an automated Buehler Automet 2000 powerhead. The samples were polished with the 3 and 1 micrometer diamond paste for 1 hour each, followed by the ¼ micrometer diamond

paste for 1.5 hours. The samples were polished in increments of 15 minutes and the direction of the revolving head was changed after each increment. The samples were then cleaned with ethanol and placed under vacuum until ready to be analyzed with SEM.

All samples were coated and placed into a Quanta 650 FEG variable pressure SEM with an automated backscattered electron detector. The accelerating voltage was 30 kV. Bruker XFlash® Detector 5010 energy dispersive spectroscopy (EDS) was used to identify phases with the sample. All images were run at a 5.0 spot size with a 3 microseconds dwell time. Samples that were obtained before and after the exposure period were compared in terms of presence and distribution of TiO_2.

3.5 MONITORING OF FIELD SITES

In addition to being observed before and after exposure, the three field sites were monitored every three months using several different techniques. Weather data were recorded to understand how rainfall, solar radiation, and other factors affect performance of the photocatalytic coatings. Onset Hobo weather stations were placed at the Austin and Houston field sites, and a Campbell Scientific weather station was placed at the JJ Pickle field site. All of the weather stations recorded rainfall, temperature, relative humidity, solar radiation, wind speed, and wind direction.

3.5.1 Ion Chromatography

Water samples were obtained before, after, and every three months throughout exposure by washing the concrete specimens with deionized water. Deionized water was used to be sure no trace amounts of nitrate or nitrite ions were present before contact with the concrete. The deionized water was placed into a clean and unused 2-gallon capacity pump sprayer. 2 liters of deionized water were then pumped and sprayed in a steady

stream onto the coated concrete surfaces, as shown in Figure 3.12. This volume was selected because it is approximately equal to a 1 in. rainfall over the surface of the specimen.

Figure 3.12: Concrete Washing Procedure

This process was repeated for each of the four sections of the barrier specimens and each of the slab specimens. Each of the water samples was collected in an aluminum dish and transferred to plastic bottles using a funnel. The samples were then capped. Figure 3.13 shows the collection procedure.

Figure 3.13: Water Collection Procedure for Concrete Specimens

The samples were transported back to the lab. Each sample was weighed and then divided in half, and the half-samples were weighed again. One of the halves was stored and the other was uncapped and placed in a vacuum oven. Each sample was evaporated until it reached a volume close to or just above the volume necessary for ion chromatography testing, which was approximately 150 milliliters. The purpose of evaporation was to concentrate the samples in order to be better able to detect nitrate and nitrite concentrations near or below the minimum detection limit. Figure 3.14 shows the vacuum oven drying process.

Figure 3.14: Ion Chromatography Sample Evaporation

Approximately 150 milliliters of each sample was sent to Water Testing USA in Cleveland, Ohio for evaluation for the presence of nitrate and nitrite ions using ion chromatography. As described in Chapter 2, the presence of nitrate and nitrite ions can indicate photocatalytic activity. Water Testing USA has a minimum detection limit of 0.5 mg/L for nitrate and nitrite tests.

3.5.2 Spectrophotometry and Photography

Each of the barrier sections and slabs was monitored for changes in color and appearance using two different methods. Color was measured before and after exposure

using a Stellar Net EPP2000-HR Portable Spectrophotometer. 10 readings were taken for each specimen and averaged. By converting the transmittance of different wavelengths of light to the International Commission on Illumination (CIE) color space, color could be determined on three scales: red to green (a*), yellow to blue (b*), and black to white (L*). Three spectrophotometer readings were taken for each of the barrier sections and slabs. These readings were then averaged to determine color values. Specimens were also photographed before and after exposure to note any visual changes and the accumulation of visible dirt or discoloration.

3.5.2 Temperature

Temperature of each specimen was recorded during each site visit using an Infrared Thermometer to determine the effect of coatings on temperature of the concrete.

Chapter 4: Results and Discussion

The results obtained from the testing program described in Chapter 3 are presented and discussed in this chapter. The fresh and hardened concrete properties that were measured for quality control during the creation of concrete slab specimens are presented first. In Section 4.2 the results for specimen characterization before and after the outdoor exposure period are shown. These results include both the results for scanning electron microscopy and x-ray diffraction. In Section 4.3, exposure site monitoring results are presented. These include all data that were collected before, after, and throughout the duration of the outdoor exposure period, including ion chromatography results as related to weather data, spectrophotometry data, temperature, and general changes in appearance as observed through photography.

4.1 Fresh and Hardened Concrete Properties

Mixture designs for all concrete slab specimens were determined in accordance with that provided by Tricon Precast in the creation of highway barriers (see Appendix A). Tables 4.1 and 4.2 provide the fresh and hardened concrete properties, respectively, measured for each individual concrete mix in compliance with test methods described in Section 3.3.3.3. The results obtained for each of these properties fall in close range with those prescribed by Tricon Precast, which are included with the mixture design in Appendix A.

For some concrete mixtures, the compressive strength was measured on specimens cured in the same way as the slabs (7 days at 100% relative humidity, 14 days at 50% relative humidity). These data are presented in Table 4.3. The average cylinder

strength is slightly higher for the cylinders cured under the same conditions as the slab specimens than for the cylinders that were moist-cured the entire time.

Table 4.1: Fresh Concrete Properties

Mix #	Date	Slump (in)	Air Content (%)	Unit Weight (lb/yd^3)
1	2/9/11	3	2.5	150.4
3	2/23/11	3.5	2	146
4	3/2/11	3.5	2.4	149.6
5	3/23/11	4	4	146
6	3/30/11	5.5	2.5	150.8
7	4/6/11	4	2	150
8	4/13/11	5	2	151.2
9	5/17/11	4.5	2	146.8
10	6/6/11	4	2	148.8
11	6/8/11	5	2	150.4
12	6/14/11	6	2	149.6
13	9/13/11	4.5	2	150
14	2/28/12	6.5	2	150.8
AVERAGE		**4.5**	**2.3**	**149.3**

Table 4.2: 28-day Compressive strength of Concrete Cylinders Cured by ASTM Standard

	Max Load (lbs)							
Mix #	Cylinder 1	Cylinder 2	Cylinder 3	Cylinder 4	Cylinder 5	Cylinder 6	Average Max Load (lbs)	Average Strength (psi)
11	126,840	125,370	112,040	118,280	115,910	125,220	120,610	9598
12	120,200	116,360	123,420	122,090	125,490	118,100	120,943	9624
13	118,800	119,200	121,300	122,980	113,680	119,340	119,217	9487
14	113,570	121670	120,590	115530	110,450	115670	116,247	9251
Average Strength (psi):								**9490**
Standard Deviation:								**170**

Table 4.3: 28-day Compressive strength of Concrete Cylinders Cured by Same Conditions as Slab Specimens

Mix #	Max Load (lbs)				
	Cylinder 1	Cylinder 2	Cylinder 3	Average Max Load (lbs)	Average Strength (psi)
1	132,373	125,490	136,125	131,329	10451
3	120,970	124,840	109,065	118,292	9413
4	143,894	136,716	143,038	141,216	11238
5	140,881	141,620	137,336	139,946	11137
6	124,545	132,757	125,431	127,578	10152
7	119,493	116,776	119,139	118,469	9427
8	106,580	108,350	110,600	108,510	8635
9	121,140	123,120	126,870	123,710	9845
Average Strength (psi):					**10037**
Standard Deviation:					**894**

4.2 Specimen Characterization Before and After Exposure

Three-in. diameter cores were removed from each of the coated sections of the highway barrier before and after the one-year outdoor exposure period, as described in Chapter 3. The purpose of removing the cores was to be able to determine whether the exposure period caused a reduction in the amount or distribution of photocatalytic material. Coated sections were compared before and after exposure using scanning electron microscopy and x-ray diffraction.

4.2.1 X-ray Diffraction

X-ray diffraction (XRD) was used to analyze the composition of coated sections of concrete barriers before and after 12 months of outdoor exposure near major highways. Cores of 3-in. diameter and ½-in depth were obtained using a small coring rig. Each coated section was crushed and analyzed by XRD. The average composition of a given

section of coated concrete was analyzed, which gave information on the presence of TiO_2 and other concrete reaction products. Since the exact process was repeated on the concrete barriers after the exposure period, results could be directly compared to determine if any changes in composition had occurred as a result of the concrete being exposed outdoors. However, since the ratio of amount of coating to concrete could vary between specimens, data were not compared quantitatively.

Figures 4.1-4.4 provide the XRD analyses of all specimens before and after the exposure period for each of the four coatings tested, with major phases identified using Jade 9 software. For each of the figures, the Houston, Austin, and Lab post-exposure plots were offset in the y-direction from the pre-exposure plot by 3000, 6000, and 9000 counts, respectively. This allowed for any differences in peaks to be easily viewed (either the formation of a new peak representing a new phase or the absence of a particular phase between field sites or exposure time). Since ratios of concrete to coating vary between specimens, the presence of a peak, and not its intensity, is the important consideration for each of the plots.

Figure 4.1, which shows the XRD analysis for the uncoated section, indicates no major change in composition after the exposure period for any of the field sites. The major phases that were identified both before and after exposure were calcite, the mineral present in both aggregates used in all concrete specimens, quartz, a major component of sand, and portlandite, which is present in hydrated cement. Since TiO_2 was not applied to this surface, it is not surprising that neither anatase nor rutile were identified.

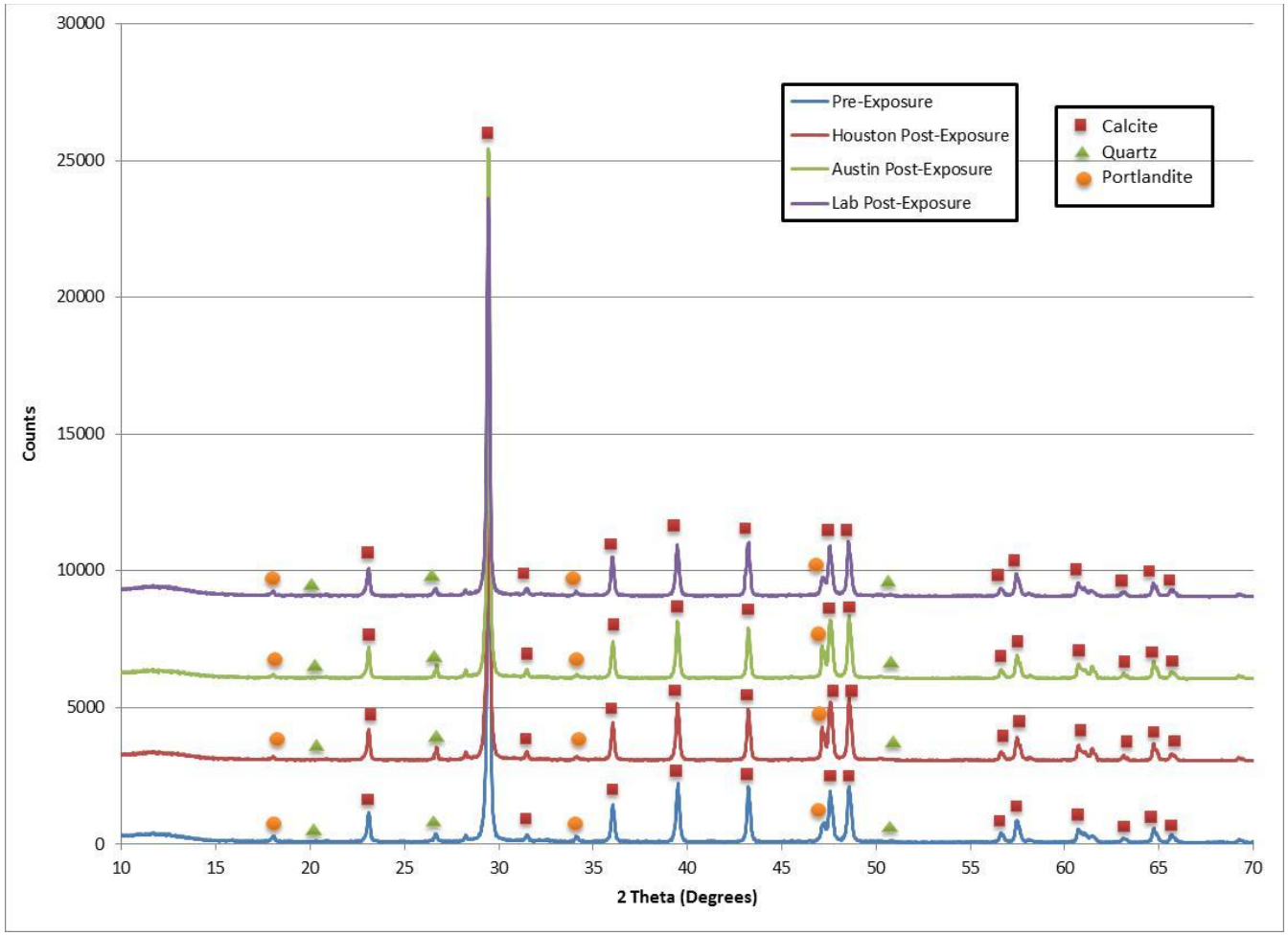

Figure 4.1: XRD Analysis of Uncoated Barrier Core Before Exposure and After Exposure in Houston, Austin, and the Lab Sites

Figure 4.2 shows the XRD analysis for the TxActive specimen. Calcite, quartz, and portlandite were again identified both before and after exposure for all field sites as components of the concrete. Both the concrete and part of the stucco matrix contained a significant amount of calcite in the form of limestone aggregate. Also identified in the pre-exposure sample were magnesite and dolomite, other phases present in the concrete. These phases were not identified in the post-exposure Houston or Lab samples but were identified in the Austin post-exposure sample, which is likely due to their relative ratio to calcite and other more prevalent phases.

Titanium dioxide in the form of anatase was found both before exposure and after exposure at each of the three field sites; however, the peaks were not consistently high enough relative to other peaks when plotted and thus do not appear as significantly in the post-exposure plots in Figure 4.2. No new phases were identified after exposure for any of the field site locations.

Samples were not compared quantitatively as the ratio of coating to concrete present in each sample was highly variable. However, it is evident from these data that the photocatalytic material in TxActive remains present after one year outdoor exposure.

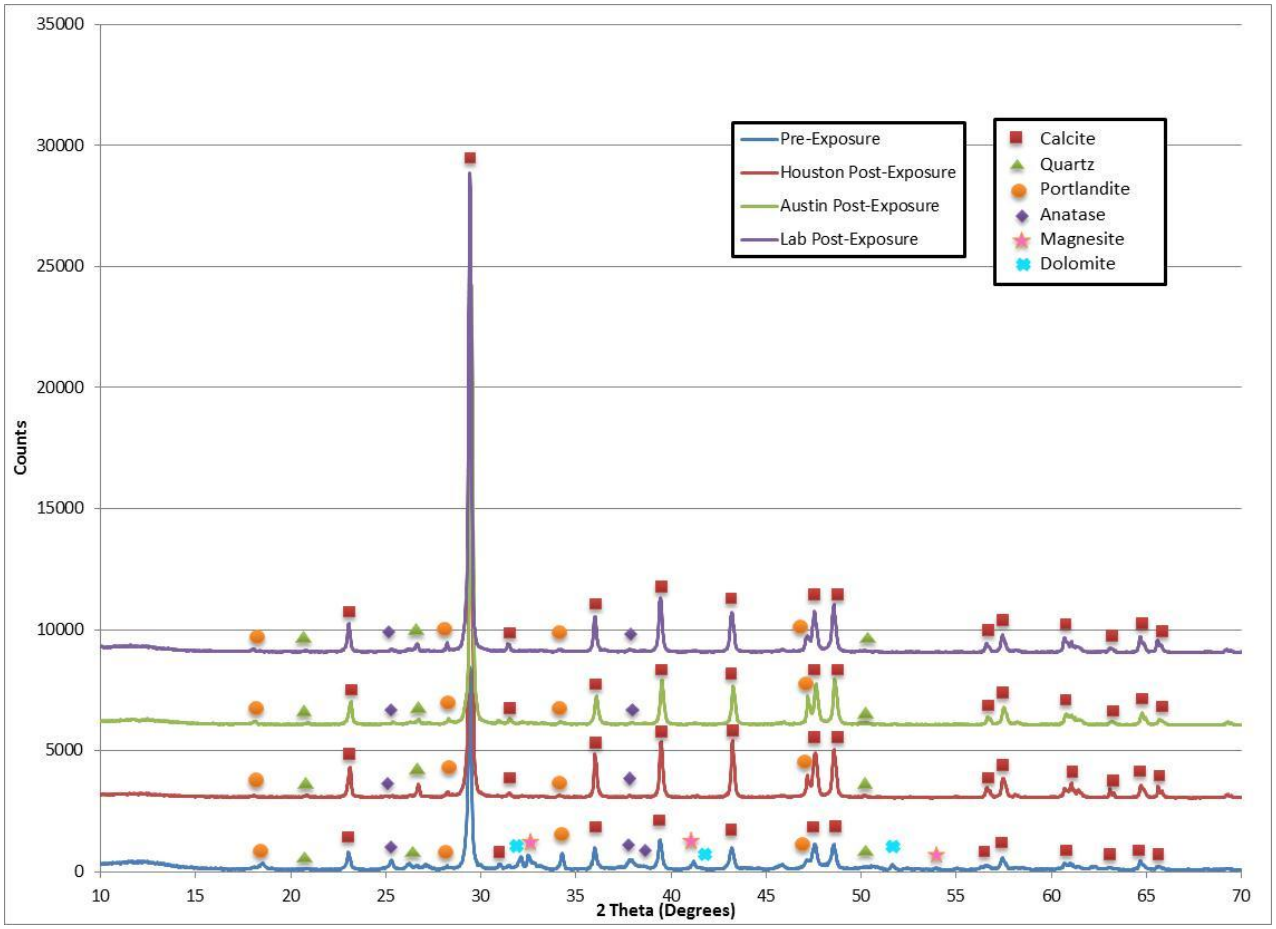

Figure 4.2: XRD Analysis of TxActive Barrier Core Before Exposure and After Exposure in Houston, Austin, and the Lab Sites

Figure 4.3 shows the XRD analysis for the Keim core. In Figure 4.4, calcite is again identified, as well as quartz, portlandite, and calcium silicate. Two major components of the Keim paint were also identified, rutile and sodium silicate (waterglass). Rutile is the active photocatalytic material in this coating. Rutile was identified both before and after exposure for each of the three field sites, so it is clear that photocatalytic material remained present after outdoor exposure.

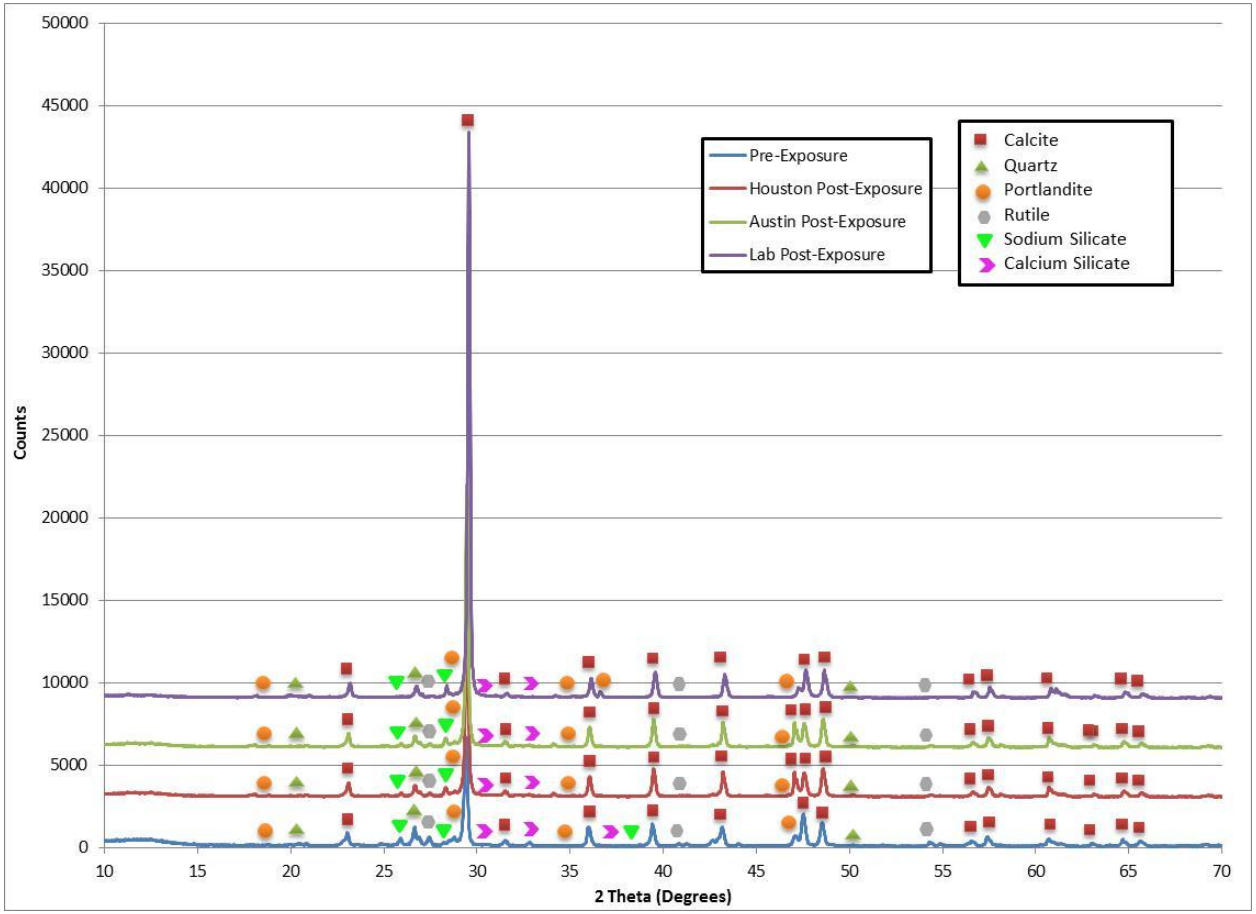

Figure 4.3: XRD Analysis of Keim Barrier Core Before Exposure and After Exposure in Houston, Austin, and the Lab Sites

Figure 4.4 shows the XRD analysis for the Pureti specimen. Calcite, quartz, and portlandite are again identified as the major phases present in the sample. Anatase was not identified either before or after exposure. This is likely due to an inadequate percentage of TiO_2 present in the sample. The Pureti coating contains less than 1% anatase by total mass, which makes it insignificant when compared to other phases, such as those present in the concrete. Because anatase was not identified at all, it is not evident from this information whether the photocataytic material degrades after outdoor exposure. There were no significant changes in composition after exposure for any of the field sites.

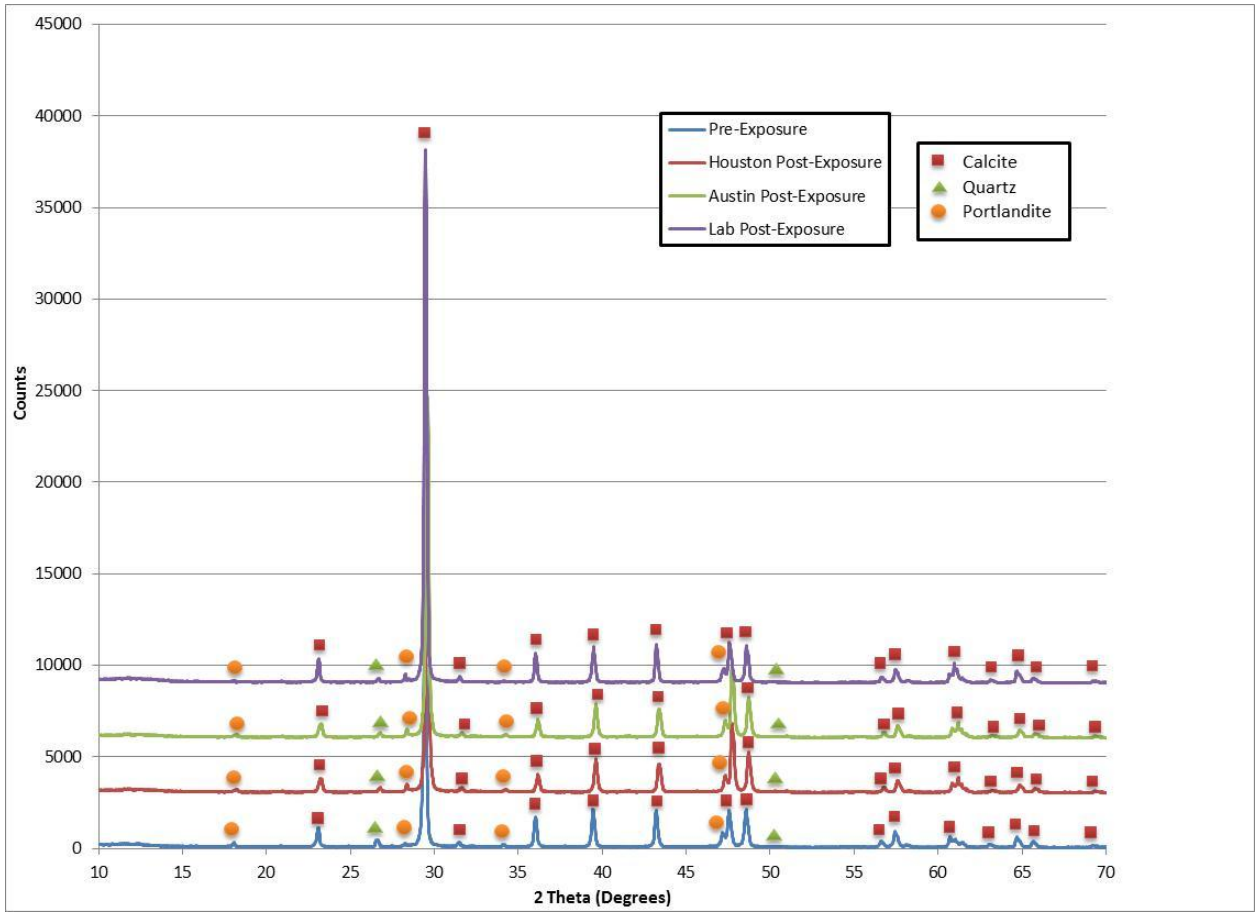

Figure 4.4: XRD Analysis of Pureti Barrier Core Before Exposure and After Exposure in Houston, Austin, and the Lab Sites

4.2.2 Scanning Electron Microscopy

In order to better understand the spatial distribution of TiO_2 in specimens exposed to outdoor conditions, scanning electron microscopy (SEM) with energy dispersive spectroscopy (EDS) was used. Cores were obtained both before and after the one-year outdoor exposure period in the manner described in Chapter 3. This technique allowed degradation of the photocatalytic coating to be monitored quite easily and effectively.

Figures 4.5-4.12 show SEM/EDS images of the uncoated and coated surfaces and cross-sections both before exposure and after exposure at each of the 3 field sites. The green color represents calcium while the red color represents titanium, which indicates the presence of TiO_2.

Figure 4.5 shows the surface of the uncoated control section of the barrier before and after exposure. The images indicate that there is a small amount of titanium present in the uncoated concrete surface. This could be due to background noise or to a small amount of titanium contained in the concrete materials. The fine aggregate material used in the mix was analyzed by XRF and found to contain 0.11% titanium. Another potential source of titanium on the uncoated section is from contamination during the coating of the adjacent Pureti-coated section.

There appears to be no significant change in the spatial distribution of TiO_2 on the uncoated section surface for any of these field site locations after the exposure period is complete.

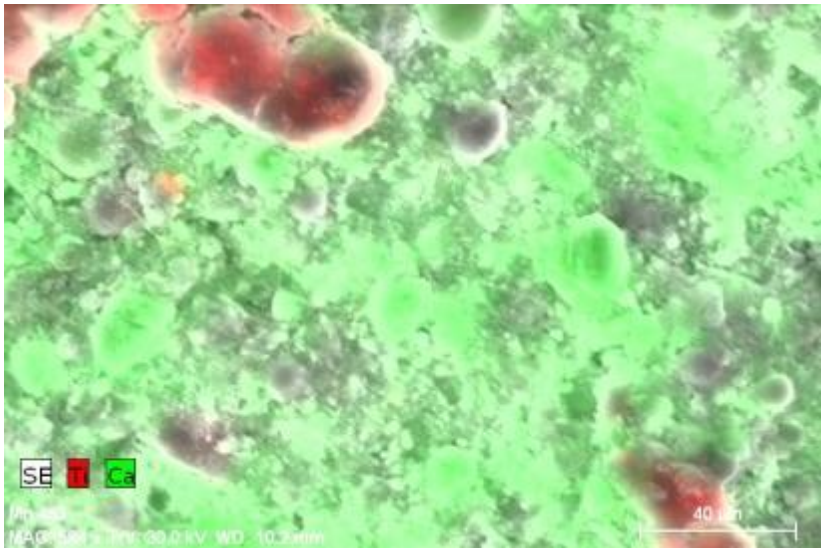

(a)

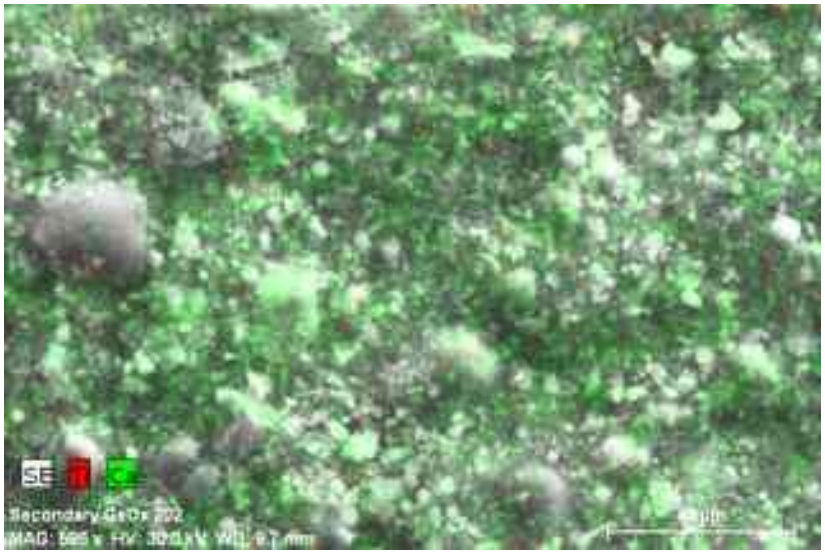

(b)

Figure 4.5: SEM Images of Control Surface (a) Before Exposure (b) After Exposure in Houston (c) After Exposure in Austin and (d) After Exposure at the Lab Site

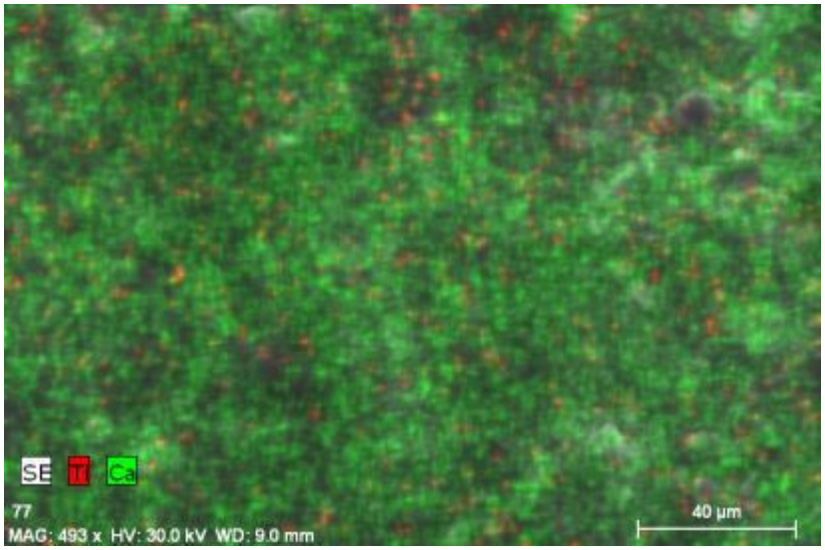

(c)

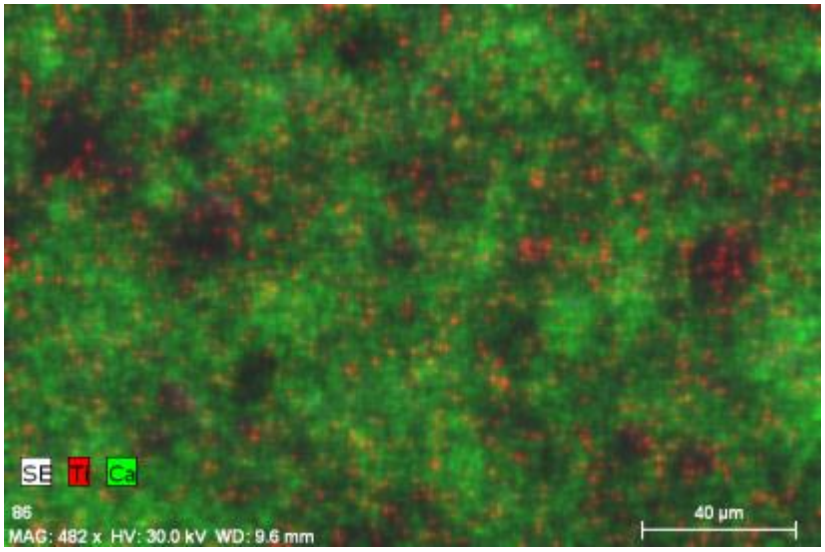

(d)

Figure 4.5, continued

Figure 4.6 shows cross-sections of the uncoated concrete surface before and after exposure. The image shows that there is an insignificant amount of titanium present at the surface of the sample, which is to be expected since a photocatalytic coating was not

applied to this section. Again, any titanium that does appear can likely be attributed to background noise associated with the imaging system.

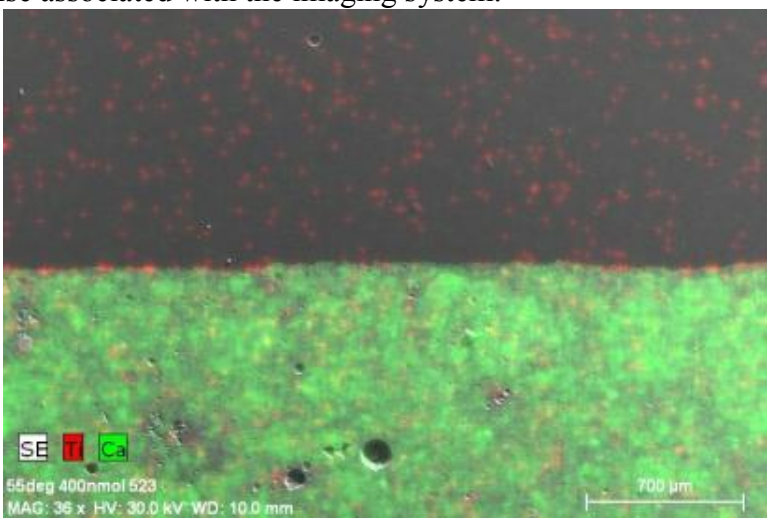

(a)

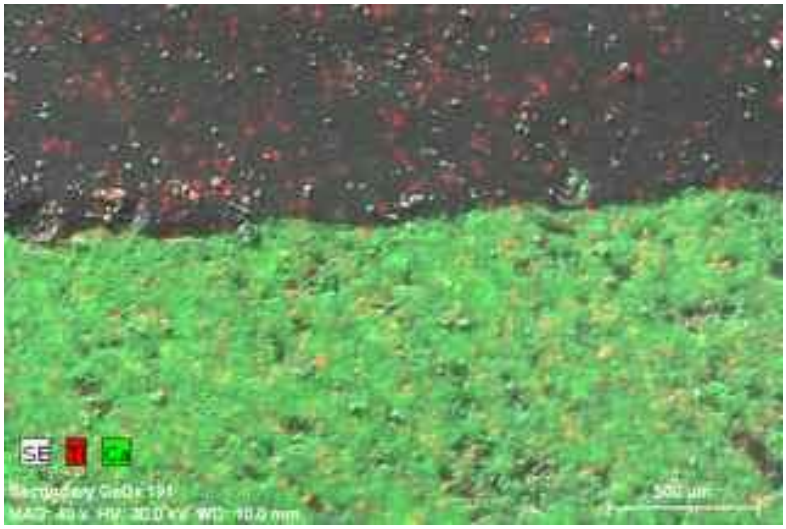

(b)

Figure 4.6: SEM Images of Control Cross Section (a) Before Exposure (b) After Exposure in Houston (c) After Exposure in Austin and (d) After Exposure at the Lab Site

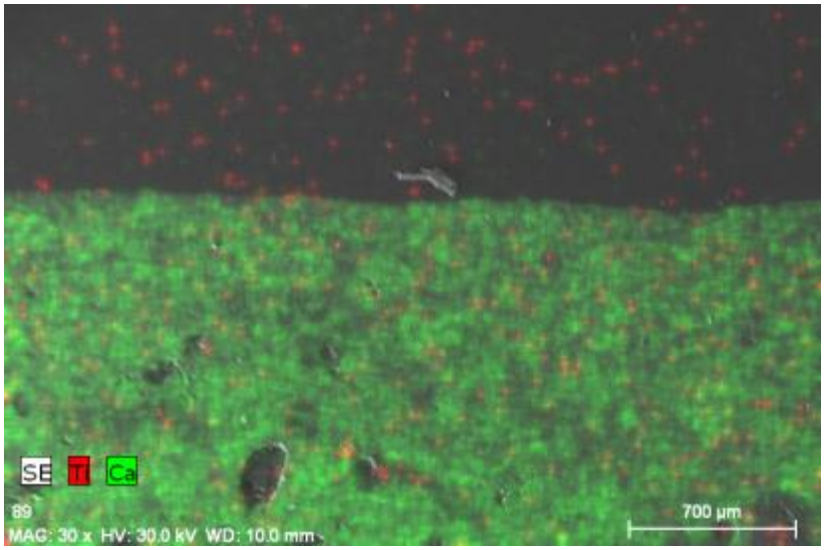

(c)

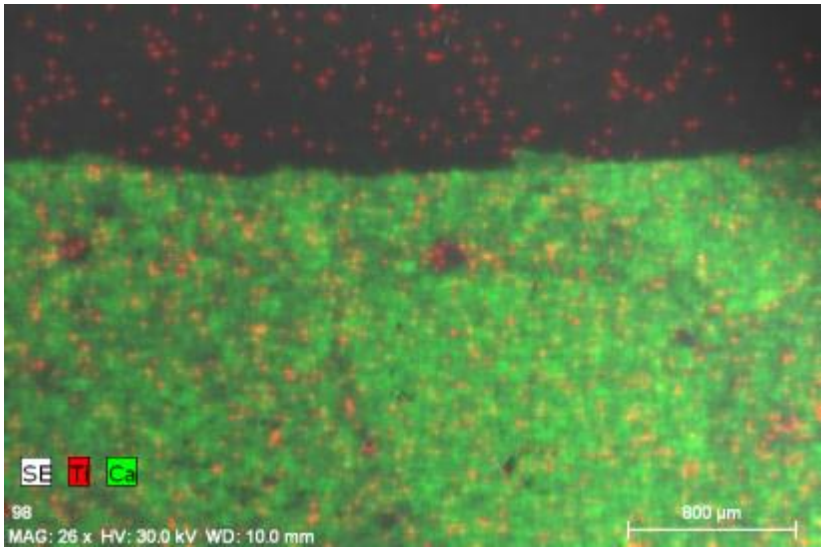

(d)

Figure 4.6, continued

Figures 4.7 and 4.8 show the barrier specimens that were coated with TxActive stucco cement. Figure 4.7 shows the surfaces of the stucco while Figure 4.8 shows cross-sections of the coated material. In both cases, the photocatalytic TiO_2 material appears to

be interspersed in small agglomerations throughout the stucco matrix, which is largely composed of limestone sand and cement. In Figure 4.8, the sand particles can be viewed as large green sections with titanium interspersed between them. There appears to be no difference in composition between the sections obtained before exposure and those obtained after exposure in any of the 3 field sites. This indicates that the TxActive stucco cement did not degrade under outdoor exposure.

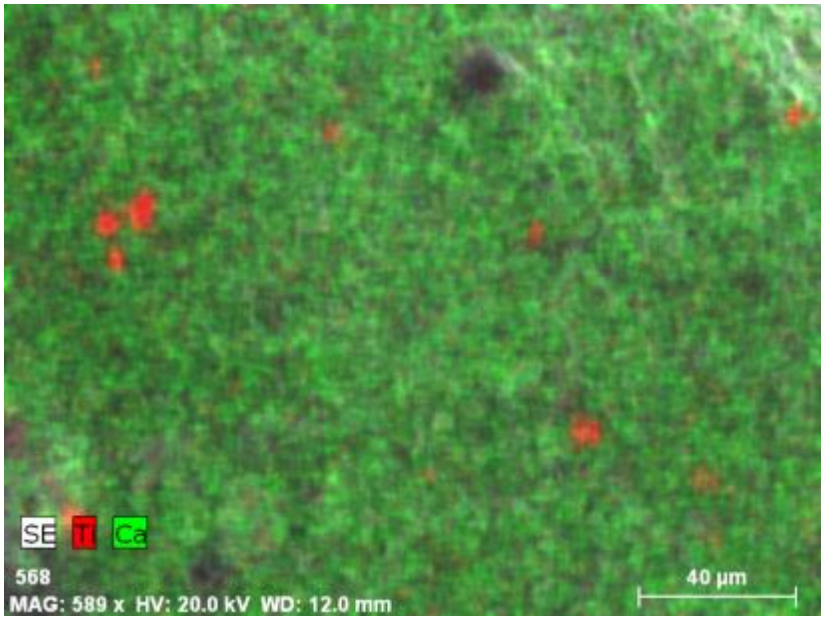

(a)

Figure 4.7: SEM Images of TxActive Surface (a) Before Exposure (b) After Exposure in Houston (c) After Exposure in Austin and (d) After Exposure at the Lab Site

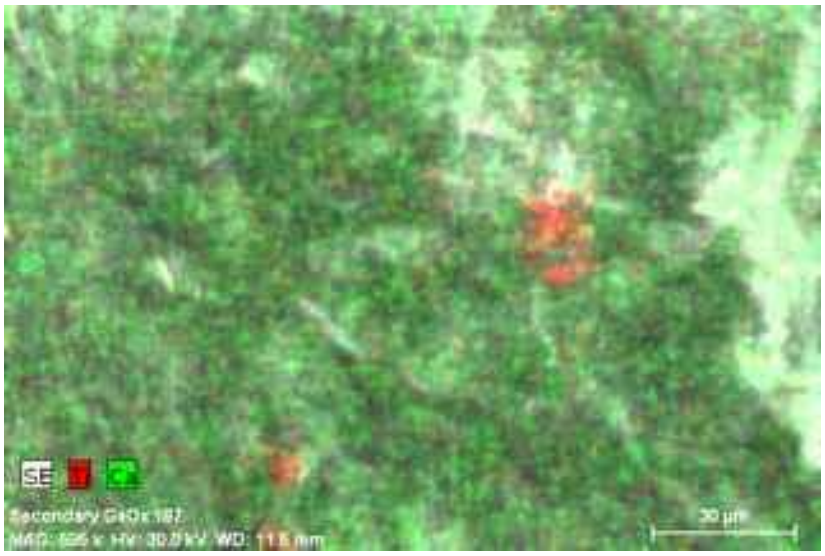

(b)

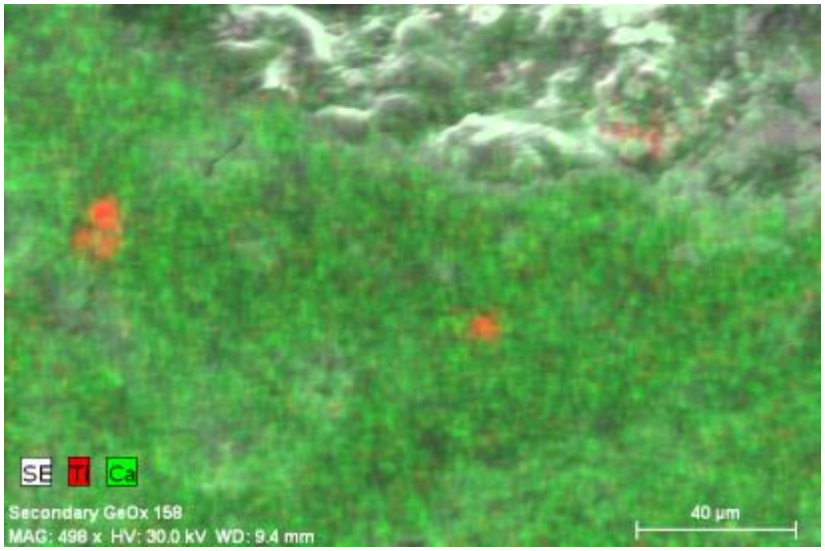

(c)

Figure 4.7, continued

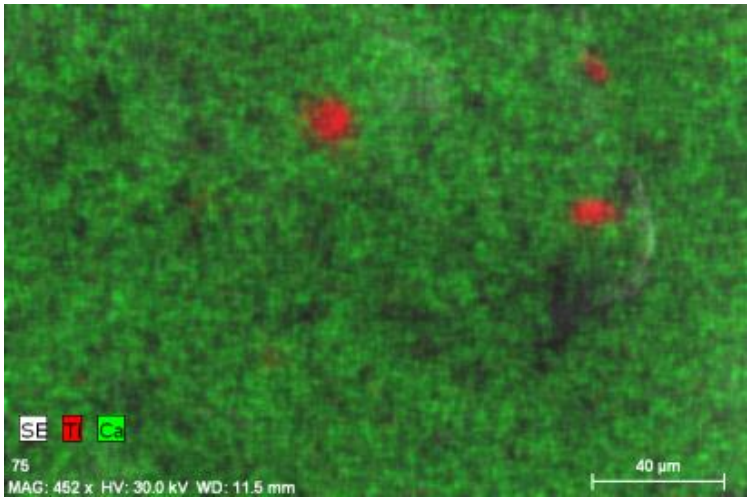

(d)

Figure 4.7, continued

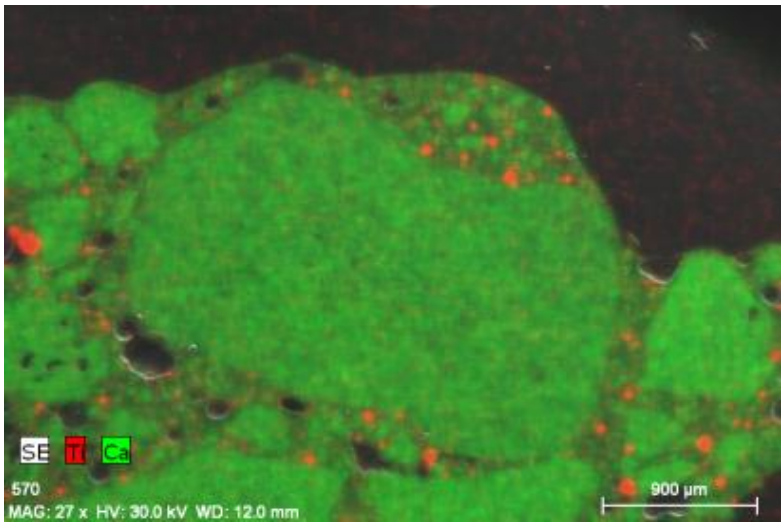

(a)

Figure 4.8: SEM Images of TxActive Cross Section (a) Before Exposure (b) After Exposure in Houston (c) After Exposure in Austin and (d) After Exposure at the Lab Site

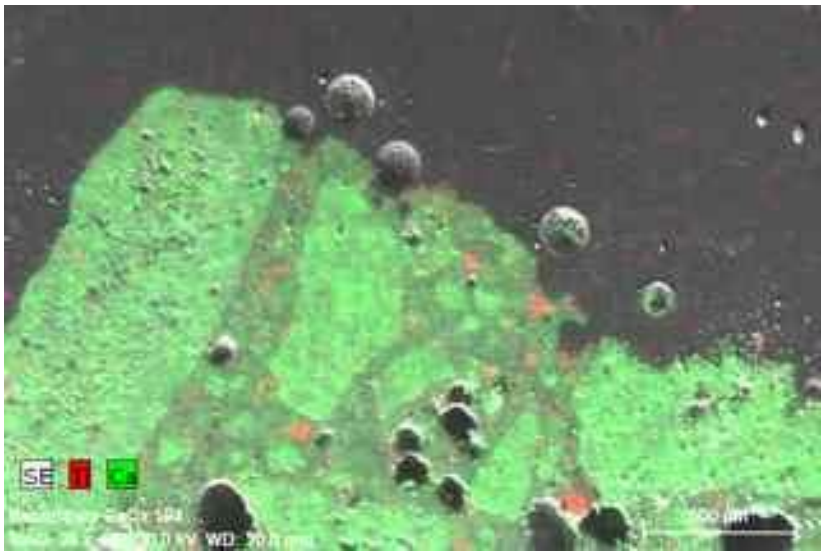

(b)

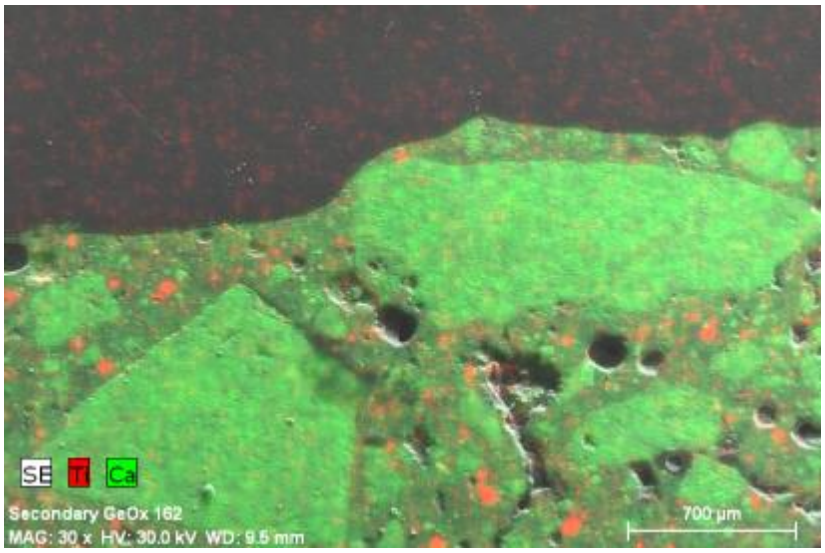

(c)

Figure 4.8, continued

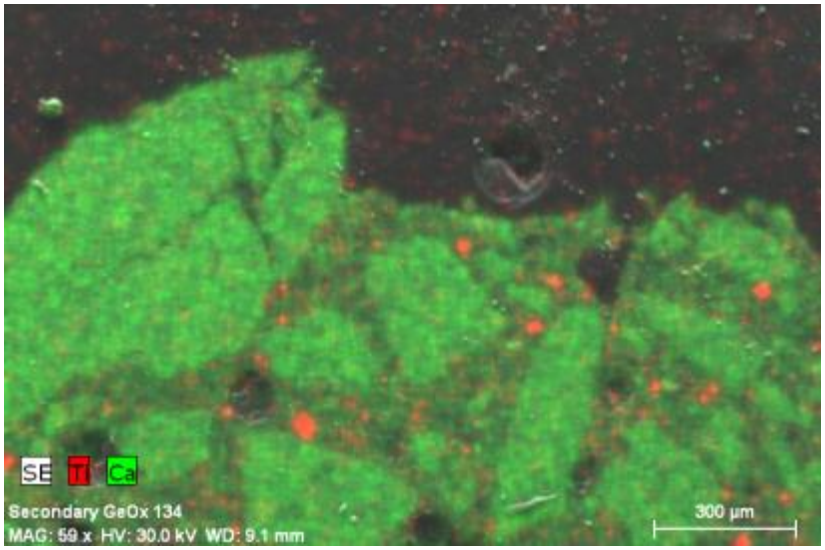

(d)

Figure 4.8, continued

Figure 4.9 shows surfaces of cores obtained from the barrier sections painted with Keim Soldalit-ME both before and after outdoor exposure at each of the 3 field sites. As expected, Figure 4.9 shows that the surface composition is almost entirely titanium. This result is expected because the Soldalit-ME product is intended to cover the surface and contains no calcium. There appears to be minimal or no degradation of the titanium composition after one-year outdoor exposure, which may have been indicated by an increase in the calcium that lies directly beneath the painted surface.

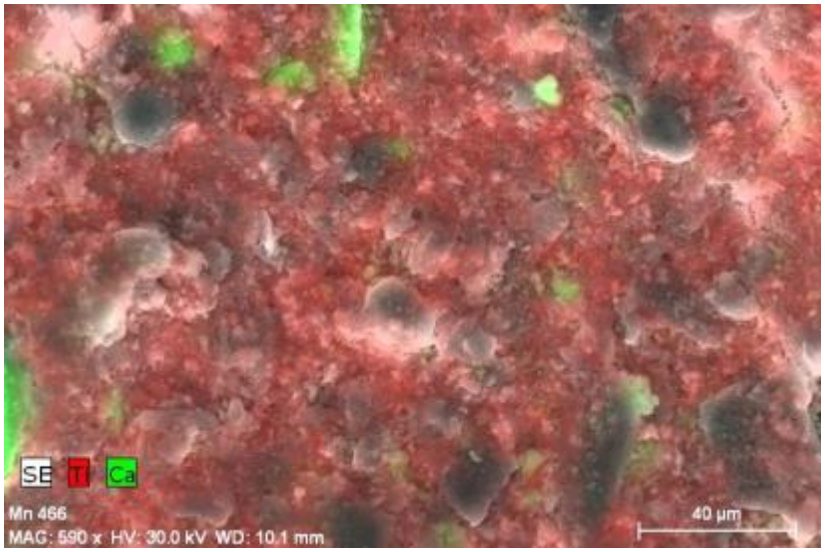

(a)

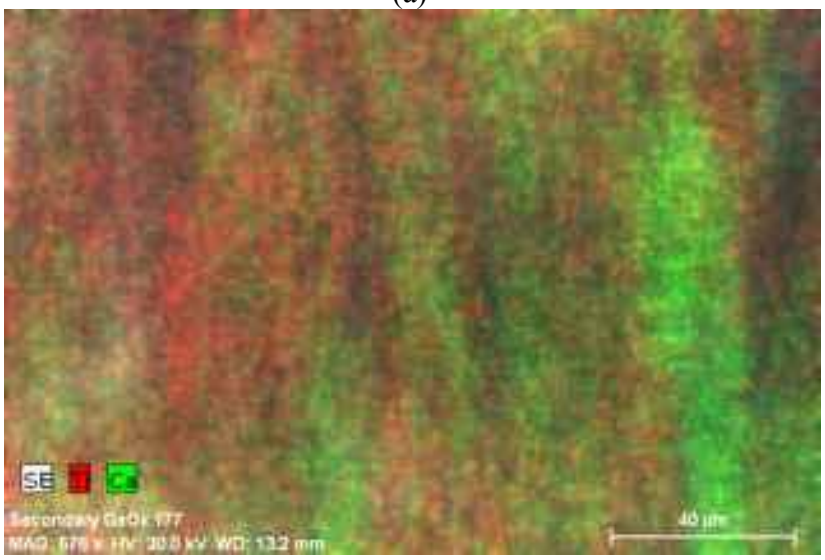

(b)

Figure 4.9: SEM Images of Keim Surface (a) Before Exposure (b) After Exposure in Houston (c) After Exposure in Austin and (d) After Exposure at the Lab Site

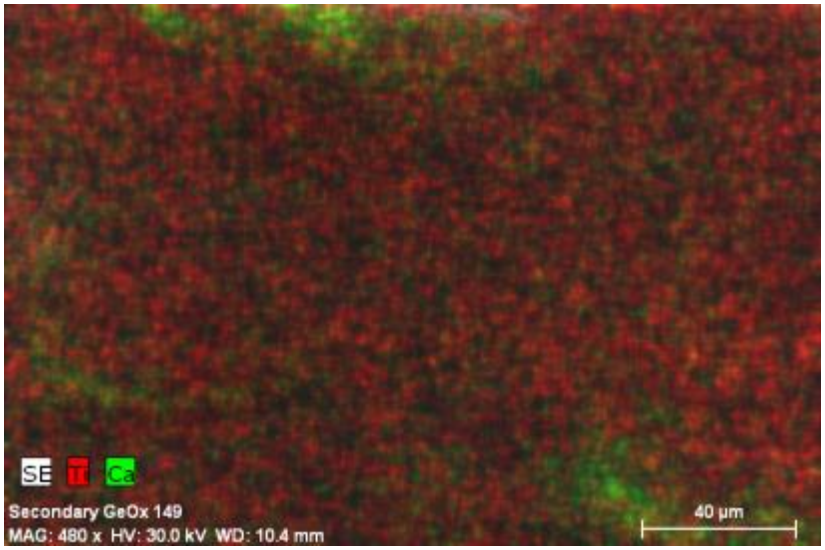

(c)

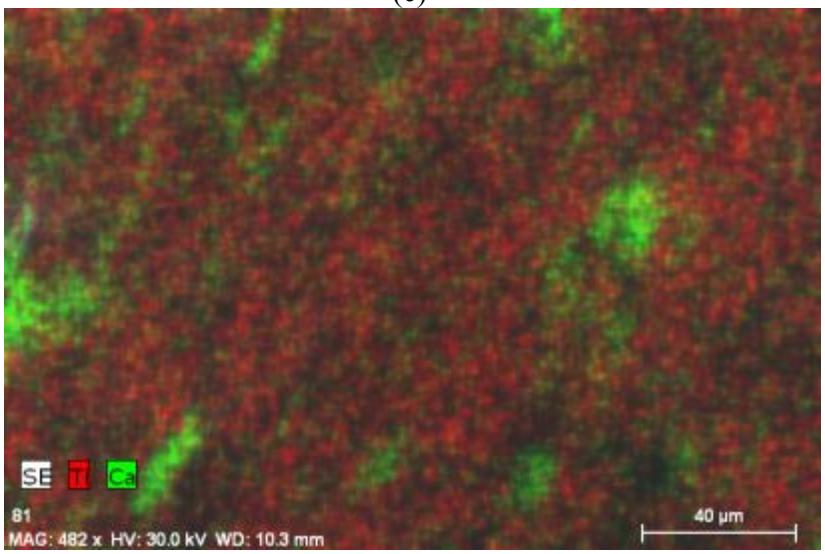

(d)

Figure 4.9, continued

Figure 4.10 shows cross sections of the Keim Soldalit-ME coated sections. The painted coating appears as a thick layer of titanium. The layer does not appear to change decrease in any of the samples taken after exposure. Therefore, KEIM Soldalit-ME paint is durable under one year outdoor exposure.

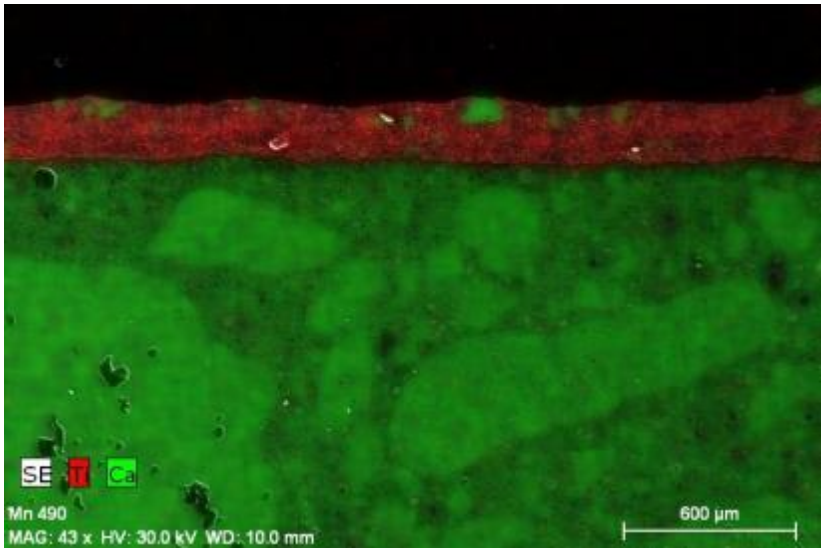

(a)

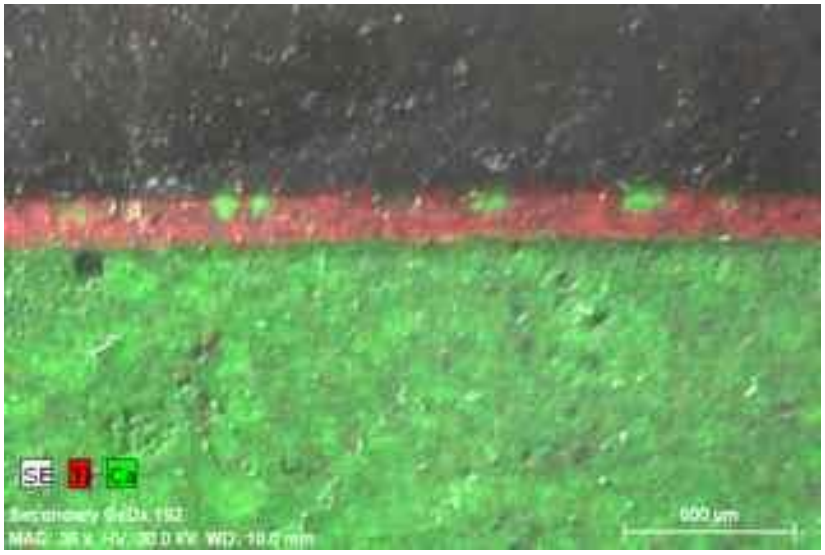

(b)

Figure 4.10: SEM Images of Keim Cross Section (a) Before Exposure (b) After Exposure in Houston (c) After Exposure in Austin and (d) After Exposure at the Lab Site

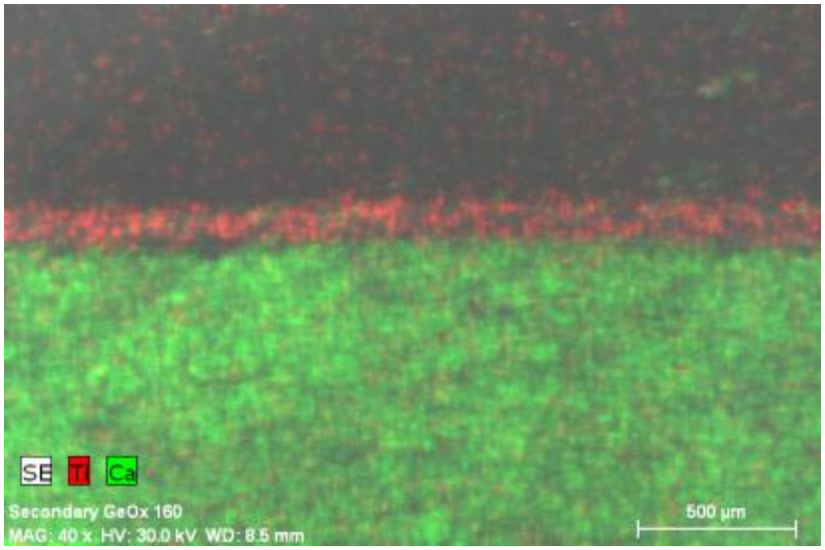

(c)

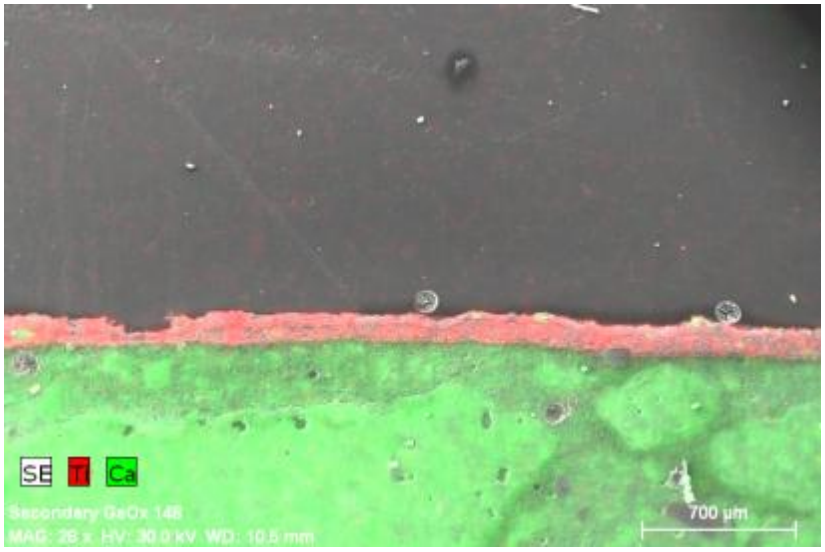

(d)

Figure 4.10, continued

Figure 4.11 shows images of the sections of the barrier that were coated with Pureti Clean. Pureti Clean is a water-based product that is sprayed on. Its spatial distribution is different from the other coatings since it is sprayed and not painted or

toweled in a thick layer. Since the coating is not intended to saturate the entire surface, it is expected that some calcium is present on the surface of the coated section. Drying of the coating may have caused the surface pattern that is shown in Figure 4.11a. The cracks that appear in the image may have formed during this drying process. From the additional images, it is not evident whether Pureti degrades during exposure, although in some cases the patterns or amount of titanium on the surface appear to decrease.

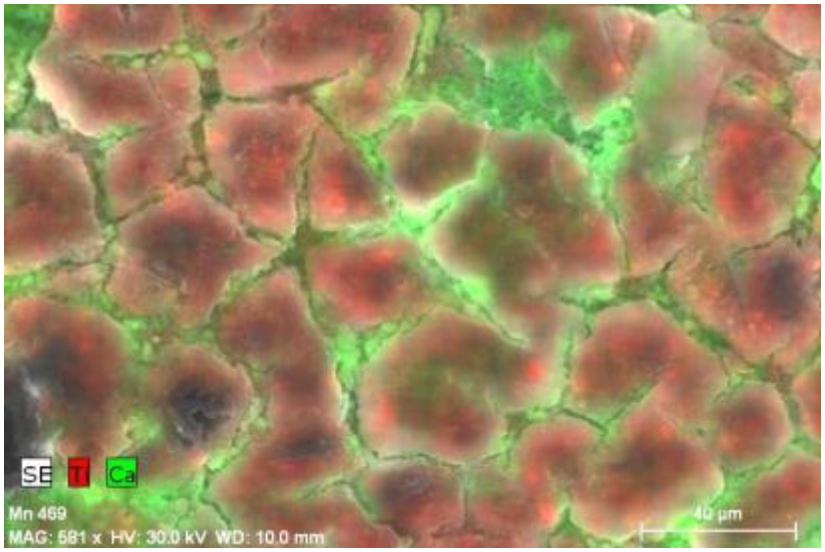

(a)

Figure 4.11: SEM Images of Pureti Surface (a) Before Exposure (b) After Exposure in Houston (c) After Exposure in Austin and (d) After Exposure at the Lab Site

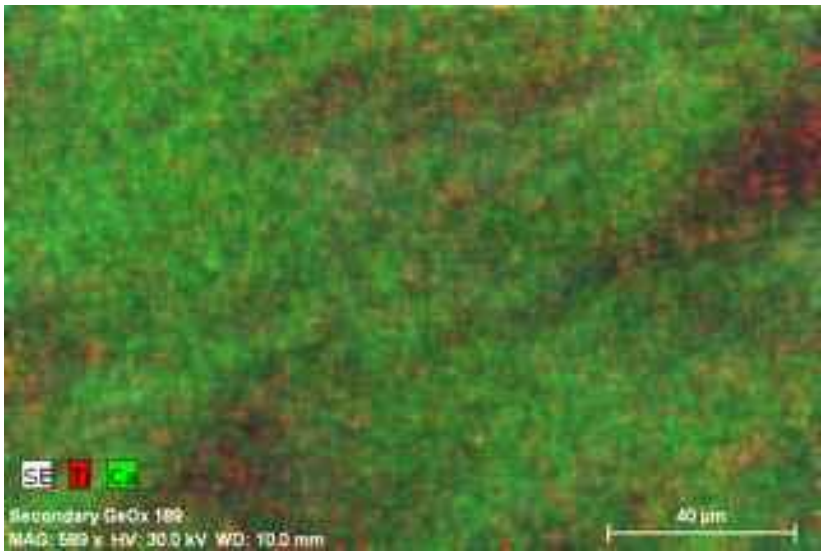

(b)

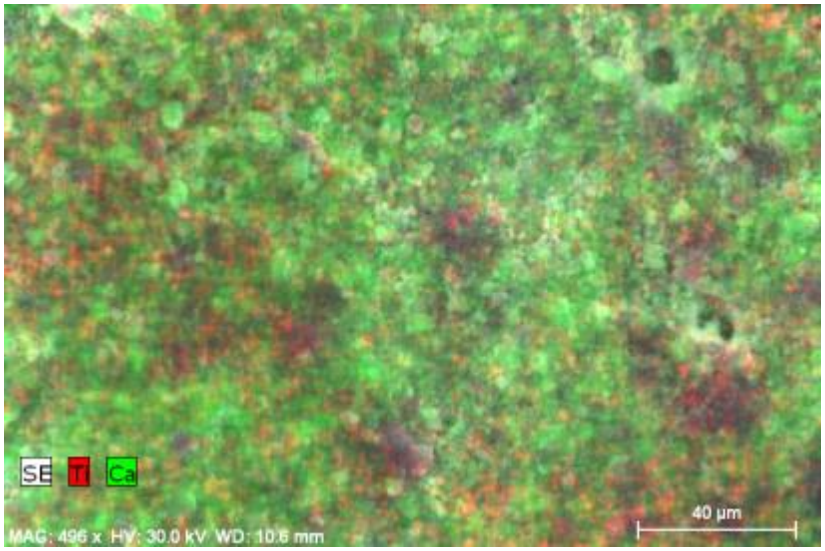

(c)

Figure 4.11, continued

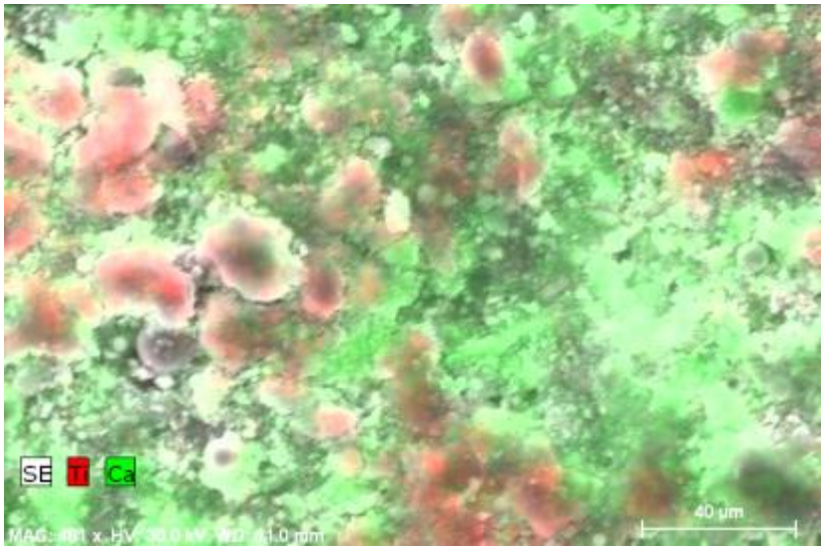

(d)

Figure 4.11, continued

Figure 4.12 shows cross-sections of the Pureti Clean coated sections. As expected, there is a thin layer of titanium present on the surface of the material where the coating was applied before the exposure period. However, it appears that the thin layer is diminished for all field sites after one year of exposure. Based on these data alone, it is possible that titanium dioxide contained in Pureti Clean is diminished due to outdoor exposure, although direct environmental testing of the coated specimens is necessary to confirm this result.

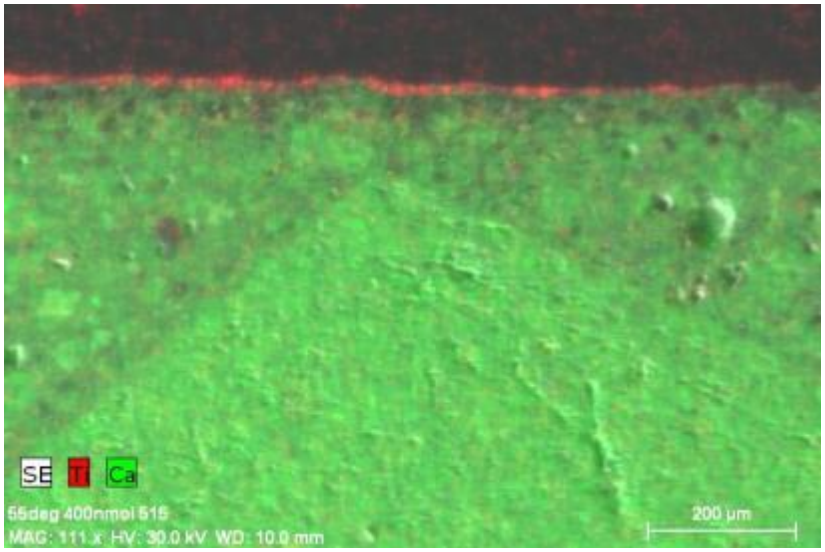

(a)

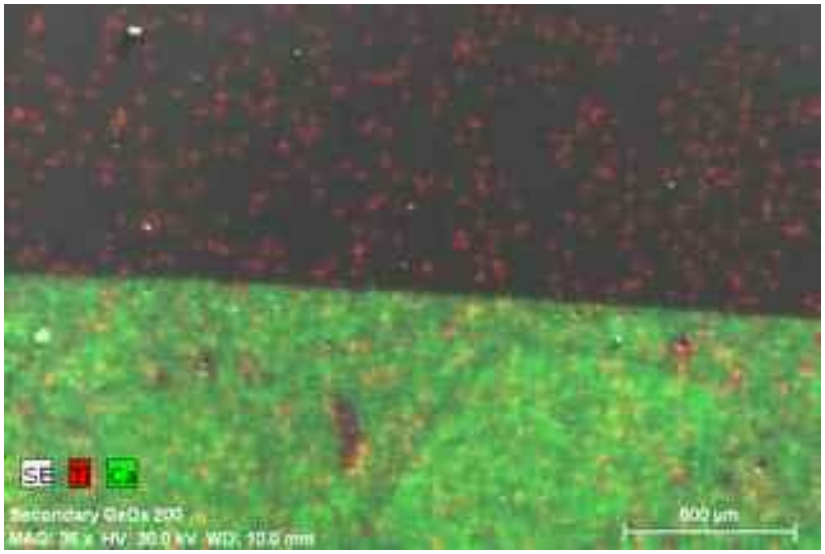

(b)

Figure 4.12: SEM Images of Pureti Cross Section (a) Before Exposure (b) After Exposure in Houston (c) After Exposure in Austin and (d) After Exposure at the Lab Site

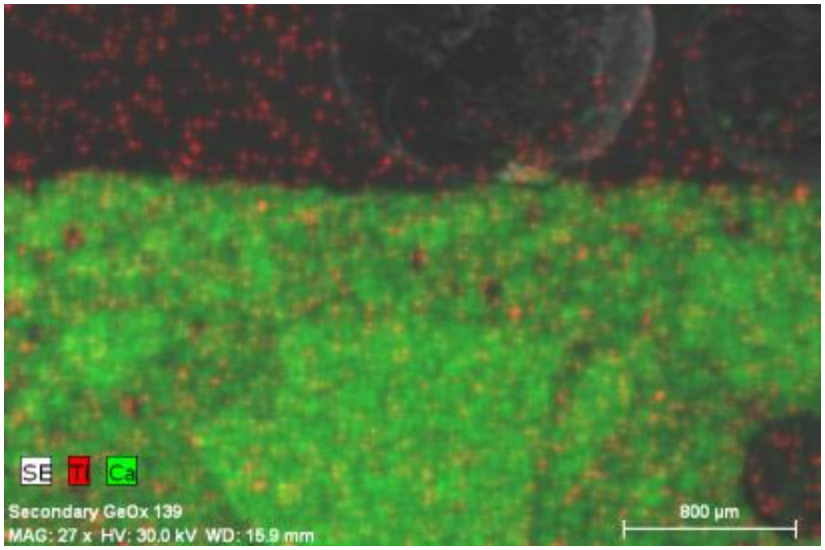

(c)

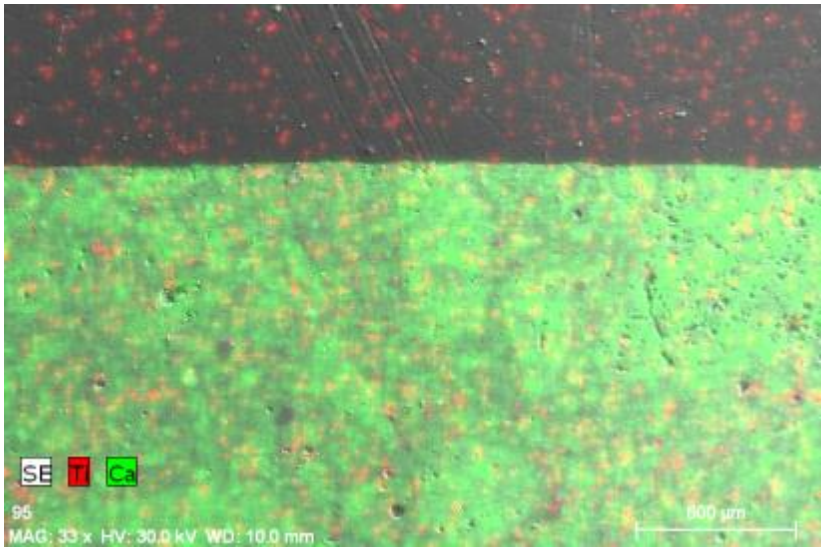

(d)

Figure 4.12, continued

4.3 EXPOSURE SITE MONITORING RESULTS

In addition to being analyzed before and after exposure using SEM and XRD, all of the coated slab and barrier specimens were analyzed before, after, and during the exposure period using several other techniques. Ion chromatography was used to understand the pollution removal efficiency of each of the specimens throughout exposure. This information was related to weather data to understand how rainfall affected pollution removal. Spectrophotometry and photography were used to examine the color and visual changes in the coated sections during the exposure period. These data were used to understand whether particulate contaminants were blocking the coatings from being exposed to sunlight. Temperature of each specimen was also measured during every site visit.

4.3.1 Ion Chromatography

All slab specimens and each of the coated barrier sections were washed with deionized water before exposure and every 3 months until the 1-year outdoor exposure period was complete in the manner described in Chapter 3. For months 0 and 3, the water was collected and analyzed. For months 6, 9, and 12, the water washes were collected and evaporated in a vacuum oven to concentrate the amount of nitrate and nitrite ions in solution. No samples were collected for the slab specimens at 12 months for any of the field sites so that they could be returned for air chamber testing in the same state. The minimum detection limit was 0.5 mg/L for the 0 and 3 month samples, and the effective minimum detection limit for the samples that were concentrated was approximately 0.15 to 0.25 mg/L, depending on the amount evaporated.

Results are reported in milligrams per liter of the original, dilute solution. All results were affected by the number of days since the last significant rainfall experienced

by the specimen during that period. Table 4.4 provides the number of days since the last significant rainfall for each site visit. These data are not available for the Austin site at 12 months due to a weather station malfunction.

Table 4.4: Number of Days since Last Rainfall for all Site Visits

Exposure Site Location	Number of days since last rainfall at time of site visit			
	3 months	6 months	9 months	12 months
Houston	17	2	5	3
Austin	20+	2	2	N/A
Lab	20+	6	5	3

Figures 4.13-4.15 present the ion chromatography results for each of the coated specimens that had significant concentrations of ions as well as the number of days since the last rainfall. These figures include data from all three field sites for initial, 3 month, 6 month, 9 month, and 1 year collections.

Figure 4.13 shows the ion chromatography results for the barrier and slab specimens that were placed at the Houston field site. The highest concentrations for the barrier were for the TxActive section at 6 months, which occurred after a period of 2 days from the last rainfall. The concentrations of these ions may indicate that this coating is removing pollutants successfully. The Pureti and Keim specimens show moderate concentrations of ions. The highest concentration for the slab specimen is again the TxActive specimen, with Pureti and Keim showing moderate ion concentrations.

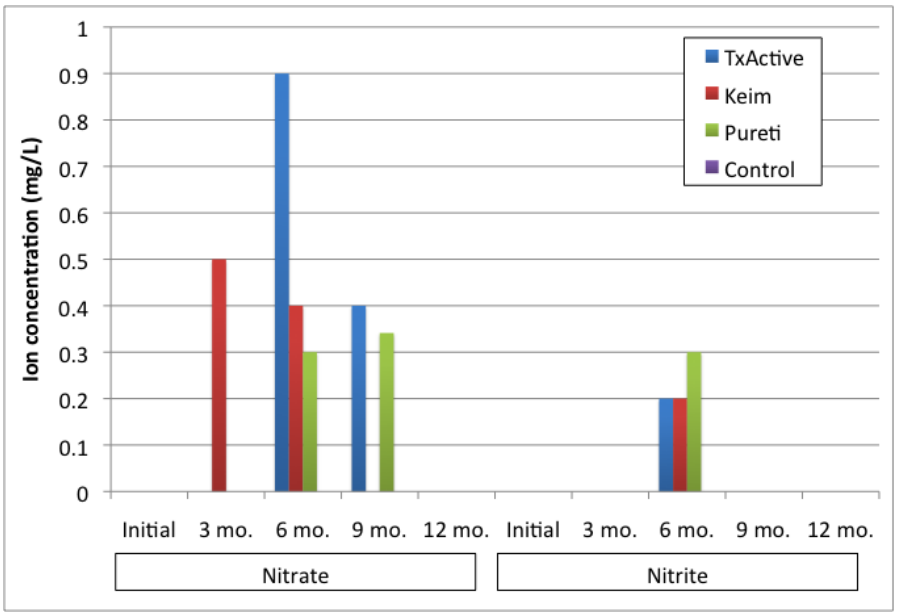

(a)

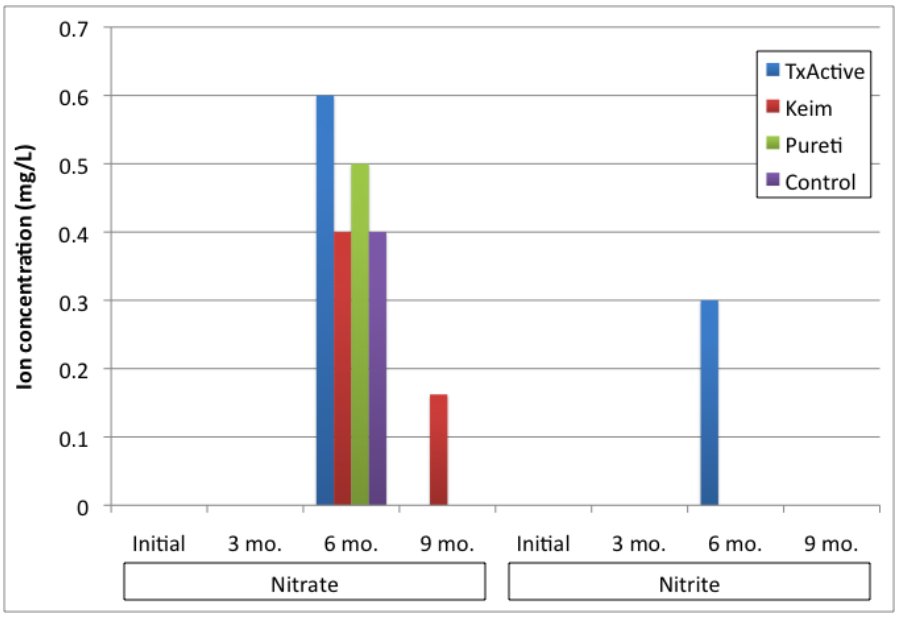

(b)

Figure 4.13: Nitrate and Nitrite Concentrations for Houston (a) Barrier Specimen and (b) Slab Specimen Wash Water

Figure 4.14 shows the ion chromatography results for the Austin slab and barrier specimens. Only the TxActive and Keim barrier sections show measurable ion concentrations for either specimen. This could be related to inadequate rainfall prior to sample collection.

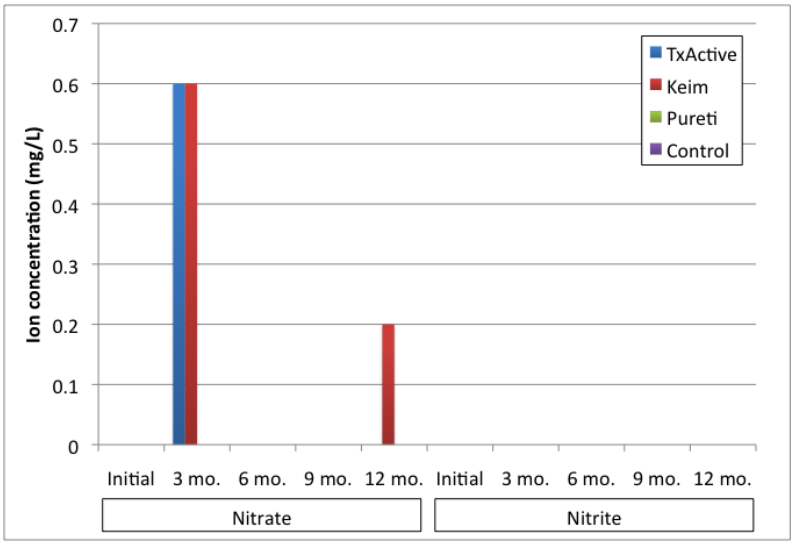

(a)

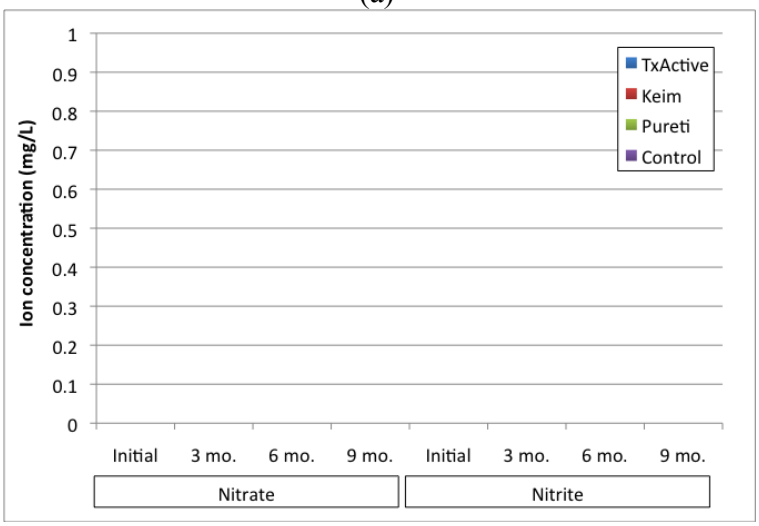

(b)

Figure 4.14: Nitrate and Nitrite Concentrations for Austin (a) Barrier Specimen and (b) Slab Specimen Wash Water

Figure 4.15 shows ion chromatography results for barrier and slab specimens for the Lab field site. For the barrier, all coatings including the control show detectable ion concentrations for the 3-month reading. That the control specimen shows measurable ion concentrations could be the result of human error or contamination from other washes. For the slab specimens, only the Keim and TxActive specimens showed measurable ion concentrations. Again, the absence of ions could be due to insignificant number of days between rainfall or another source of error.

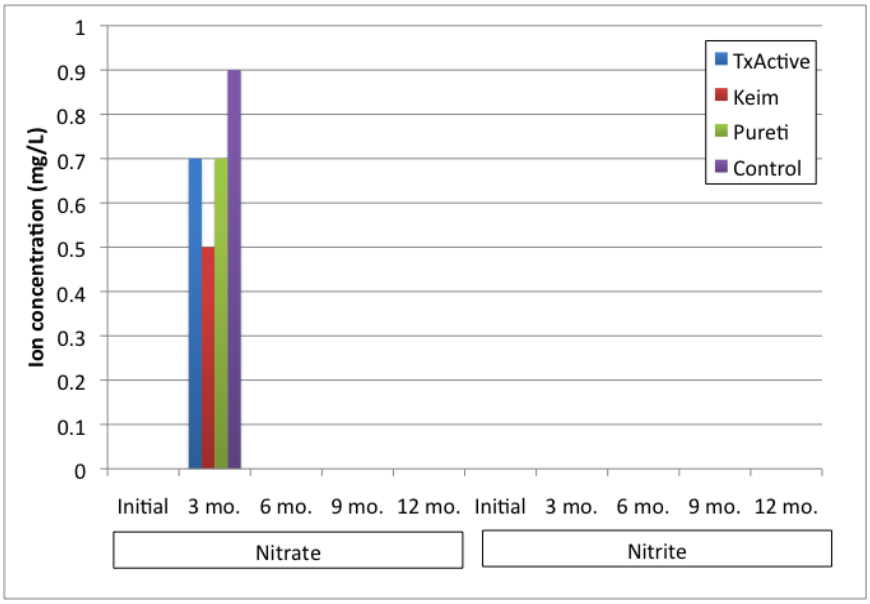

(a)

Figure 4.15: Nitrate and Nitrite Concentrations for Lab (a) Barrier Specimen and (b) Slab Specimen Wash Water

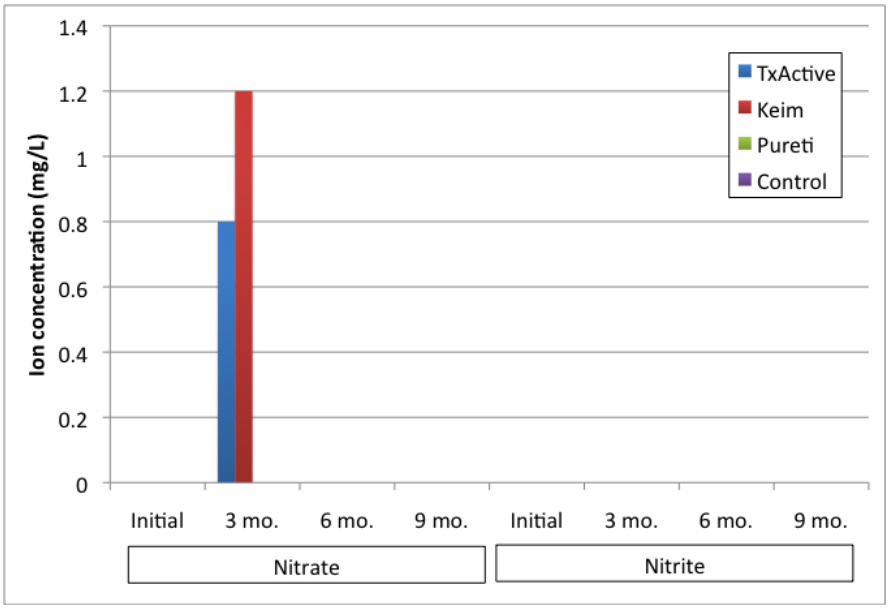

(b)

Figure 4.15, continued

Many of the results were either at or just below the minimum detection limit of testing, which was 0.5 milligrams per liter for both nitrates and nitrites. The highest overall concentration of nitrate recorded was for the TxActive barrier specimen at Houston for its 6-month reading. The TxActive slab specimen and the Pureti barrier specimen also showed nitrate concentrations above the minimum detection limit. These levels were highest for the 3 month Austin and Lab site readings and 6 month Houston readings.

Although results were lower overall than expected, there is some indication from the ion chromatography results that the TxActive and Pureti specimens, in particular, successfully removed pollution. Possible sources of error include allowing inadequate time after rainfall when sampling and low levels of solar radiation prior to sample collection.

4.3.2 Spectrophotometry and Photography

Color was measured before exposure and every 3 months throughout the duration of the exposure period using a spectrophotometer. Since photocatalytic pollution removal occurs when the material is exposed to an adequate light source, any covering of the photocatalytic surfaces with dirt, visible pollutants, or other contaminants could compromise pollution removal ability. The spectrophotometer was therefore used to determine if any contaminants were adhering to the surface by measuring any changes in color of the material over time. The most effective way to measure this parameter was through the L* scale of the CIE color space, which indicates brightness on a scale from 0 to 100, with 100 indicating bright white. This scale was particularly effective when used for the two white coatings, the TxActive stucco and Keim paint.

Figure 4.16 shows the spectrophotometer data for the TxActive barrier and slab specimens located at the Houston field site. The data presented here are the average of 10 L* readings for the sample. No data were available for the 6-month interval for the Houston site due to a computer malfunction.

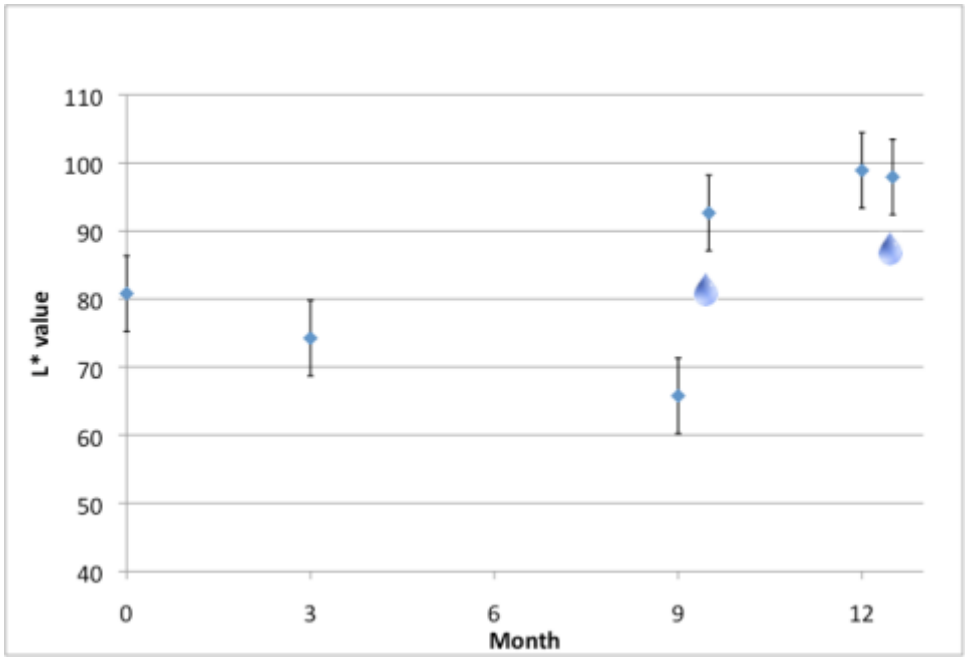

(a)

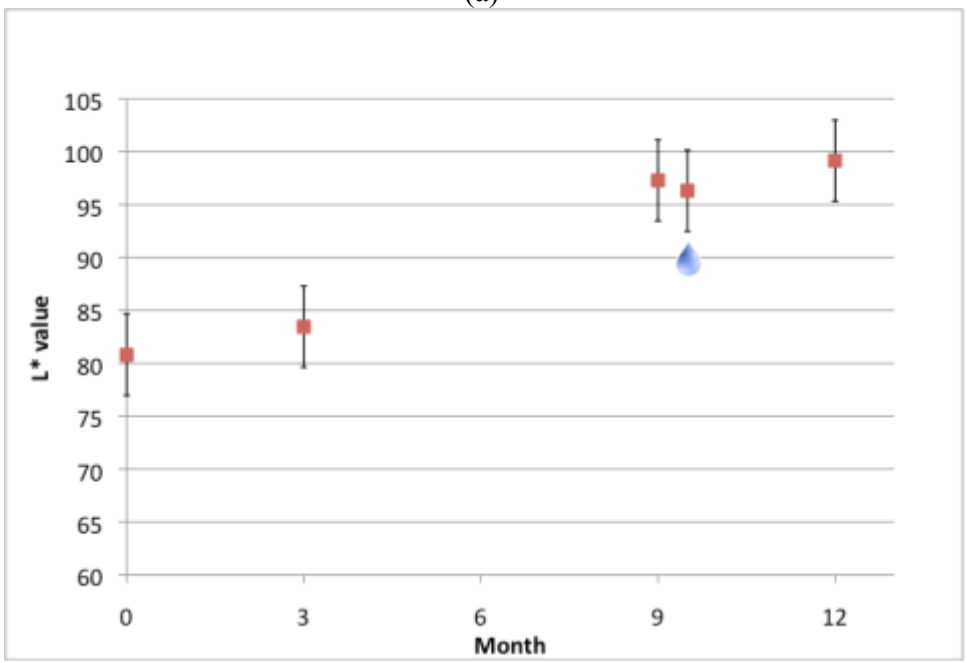

(b)

Figure 4.16: Average L* Readings for Houston TxActive (a) Barrier Specimen and (b) Slab Specimen

The data in Figure 4.16 show that although the L* reading of the specimen decreased slightly over time, this brightness was restored after washing. The coated stucco is highly variable with both bright white spots and dark, shadowed areas. This variability in color may have had an effect on L* readings recorded for these specimens. Figure 4.17 shows the spectrophotometer data for the Austin TxActive barrier and slab specimens.

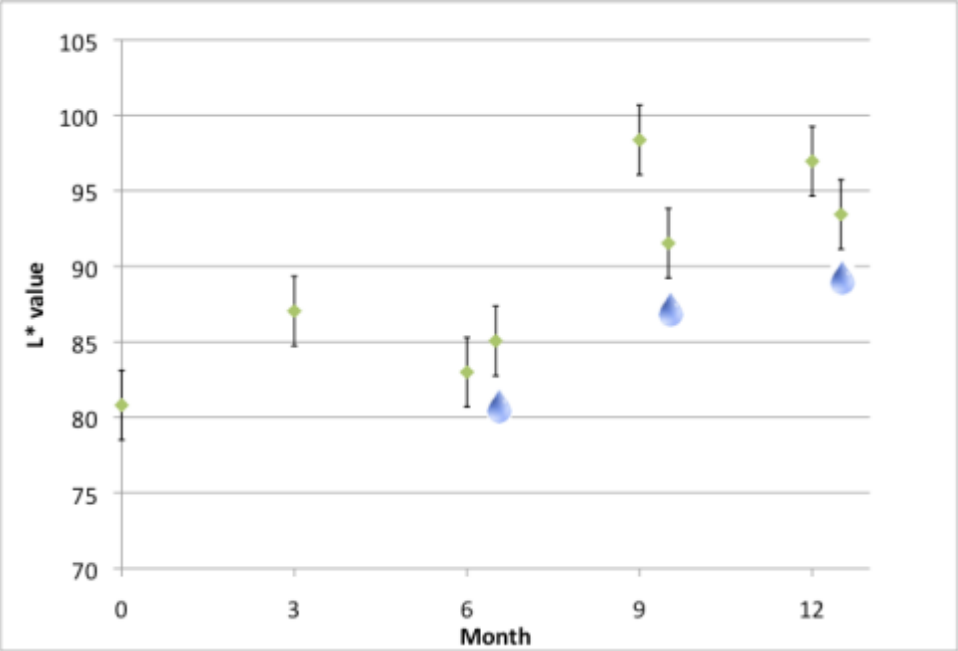

(a)

Figure 4.17: Average L* Readings for Austin TxActive (a) Barrier Specimen and (b) Slab Specimen

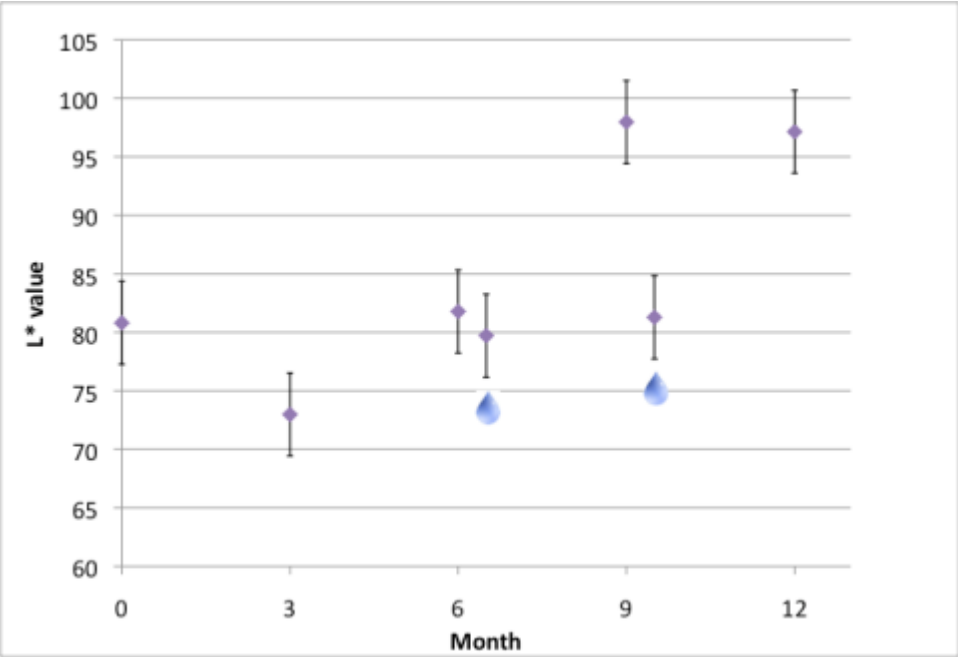

(b)

Figure 4.17, continued

Figure 4.17 shows that brightness was restored after washing during the outdoor exposure period. Although the samples lost brightness during period of low rain levels, the brightness was restored ultimately through washing. Figure 4.18 shows average L* readings for the TxActive barrier and slab specimens located at the Lab site.

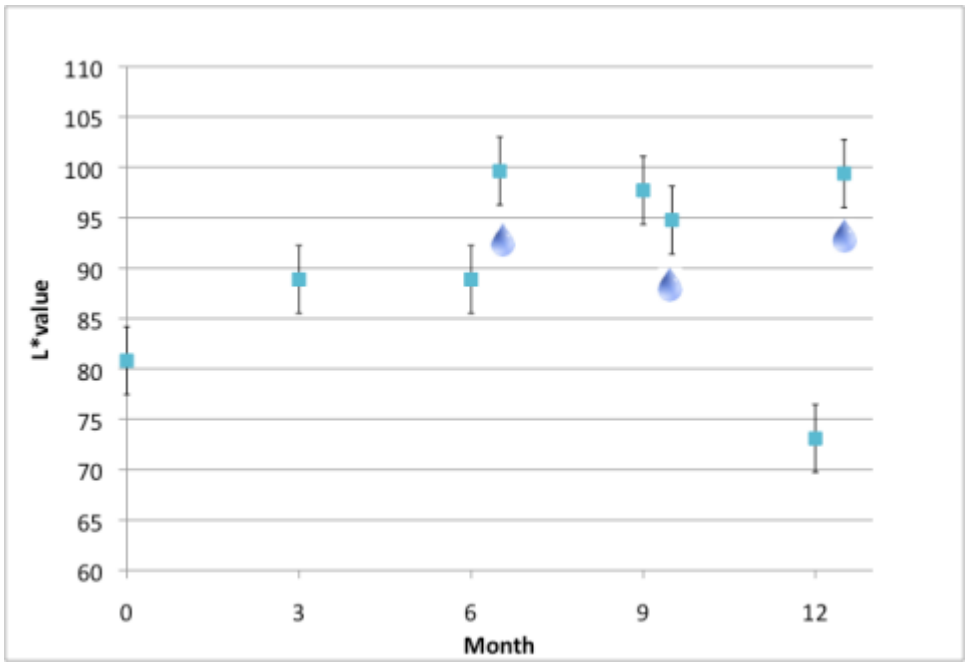

(a)

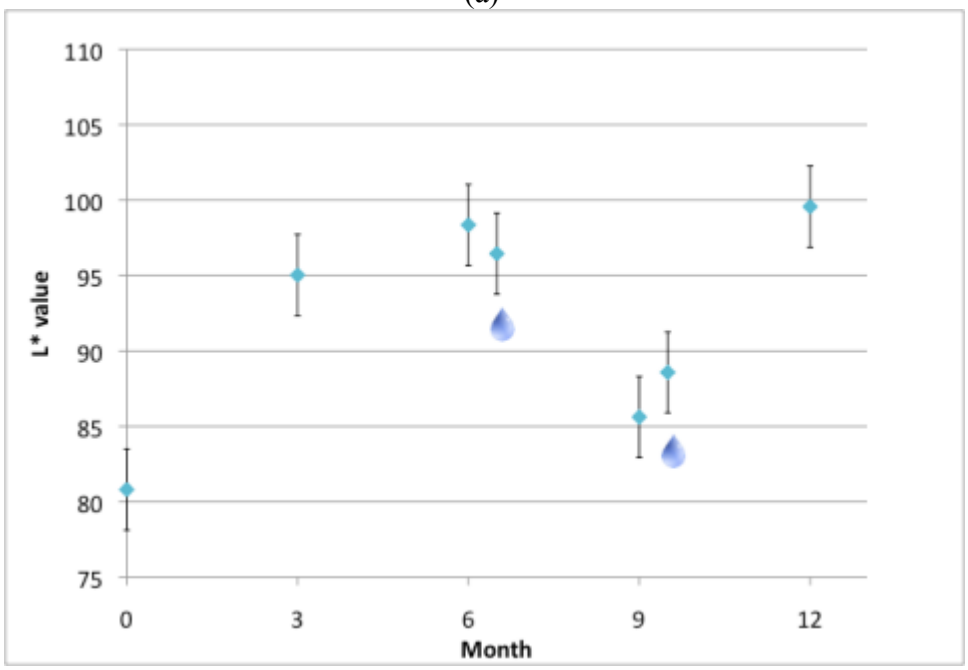

(b)

Figure 4.18: Average L* Readings for Lab TxActive (a) Barrier Specimen and (b) Slab Specimen

Figure 4.18 shows that final L* readings for both the barrier and slab specimens were higher than initial readings, indicating that brightness was not lost over time while the specimens were exposed outdoors. Figure 4.19 shows average L* readings for the Keim-coated barrier and slab specimens located in Houston.

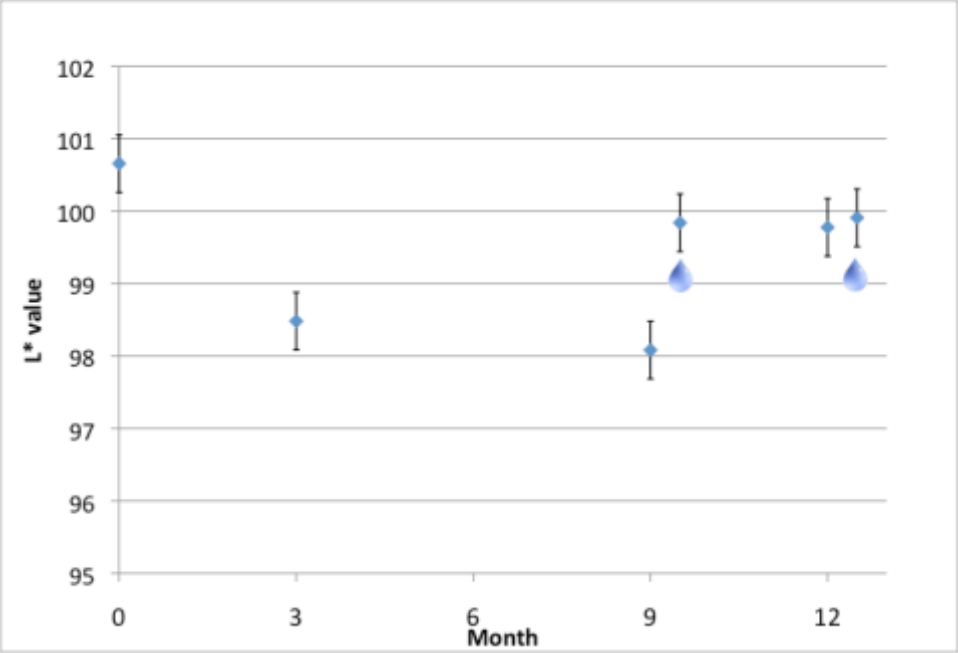

(a)

Figure 4.19: Average L* Readings for Houston Keim (a) Barrier Specimen and (b) Slab Specimen

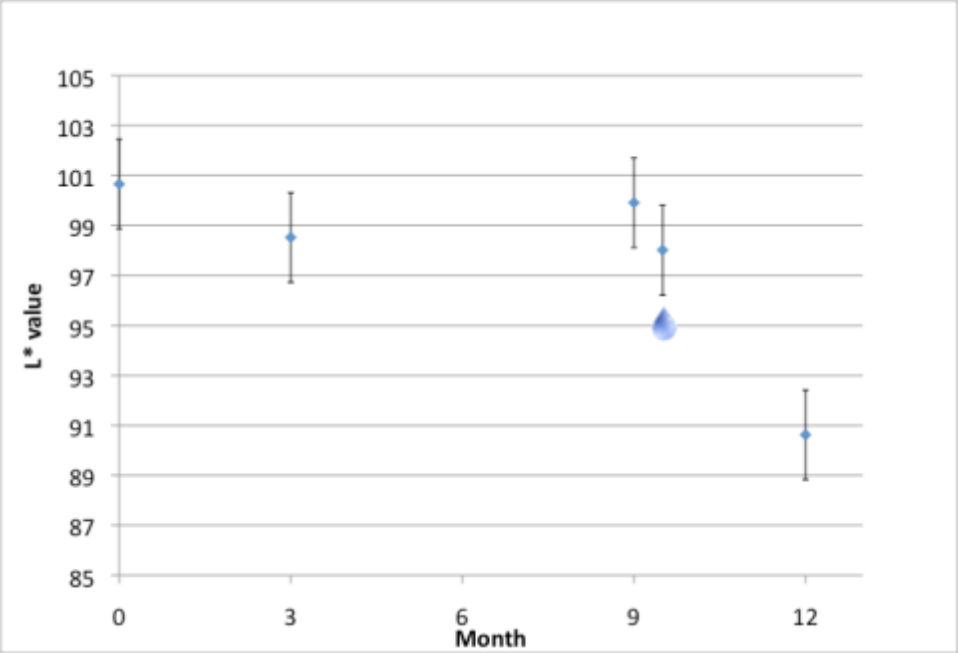

(b)

Figure 4.19, continued

For the Keim specimen, there is a slight decrease in brightness for the barrier specimen, although the final reading is within the error range of the initial reading. The final reading for the slab specimen is significantly lower than the initial reading, to the point of being outside the margin of error of the initial reading, indicating that the specimen did collect surface contaminants which darkened the specimen. From these data, it can be concluded that photocatalytic activity may be decreased due to the accumulation of these contaminants. Figure 4.20 shows average L* readings for the Keim barrier and slab specimens located at the Austin field site.

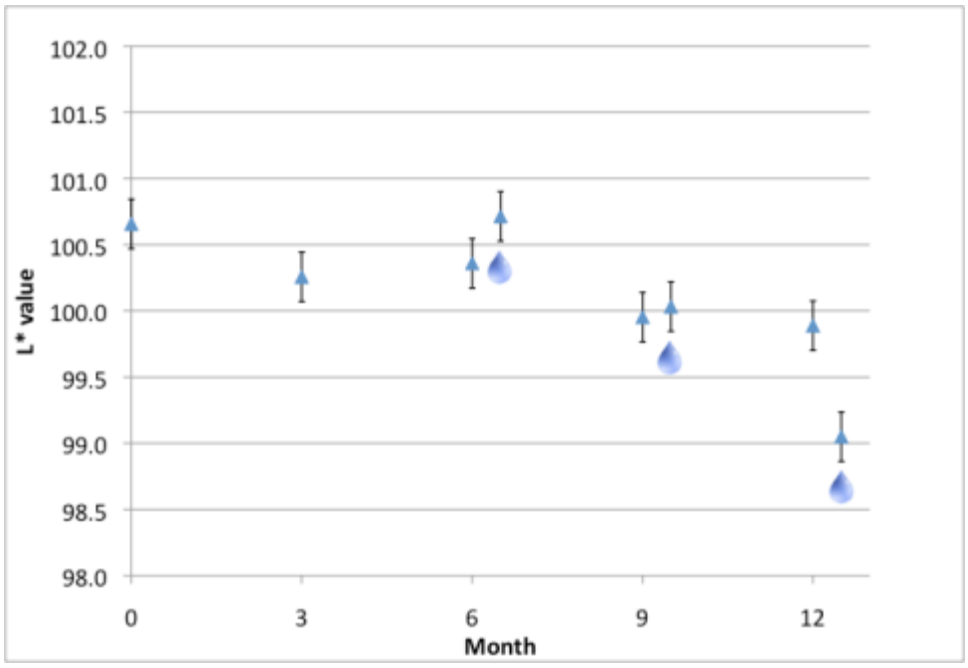

(a)

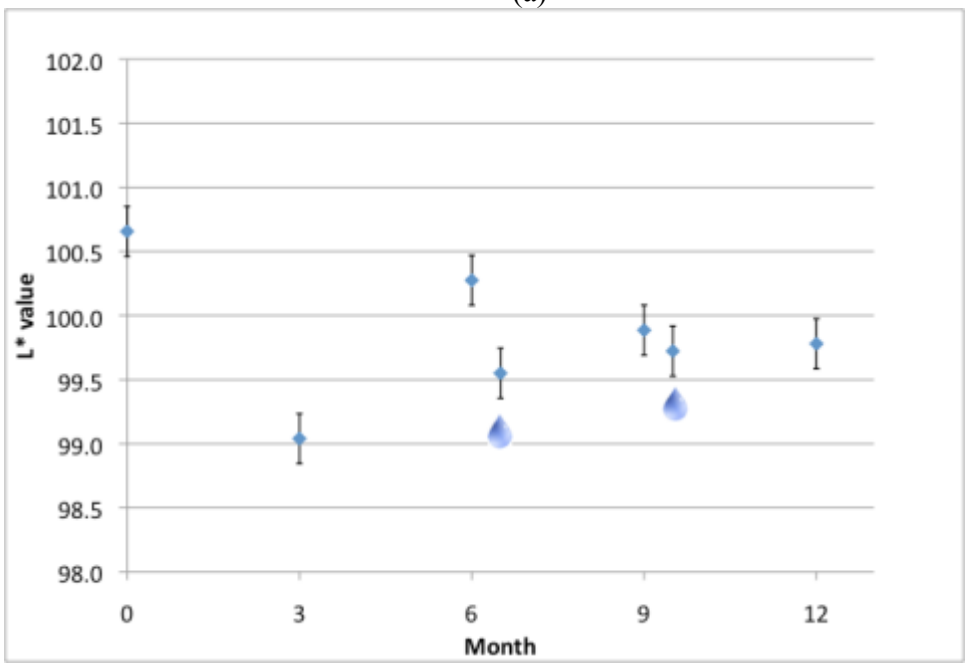

(b)

Figure 4.20: Average L* Readings for Austin Keim (a) Barrier Specimen and (b) Slab Specimen

For the Austin field site, both the Keim-coated barrier and slab specimens showed decreased L* readings for the final site visit. These decreases were outside the margin of error for both cases. This indicates that significant contaminants had accumulated on the surface, reducing the brightness of the white Keim coating. Figure 4.21 shows the L* readings over the one year exposure period for the Keim-coated barrier and slab specimens placed at the Lab site.

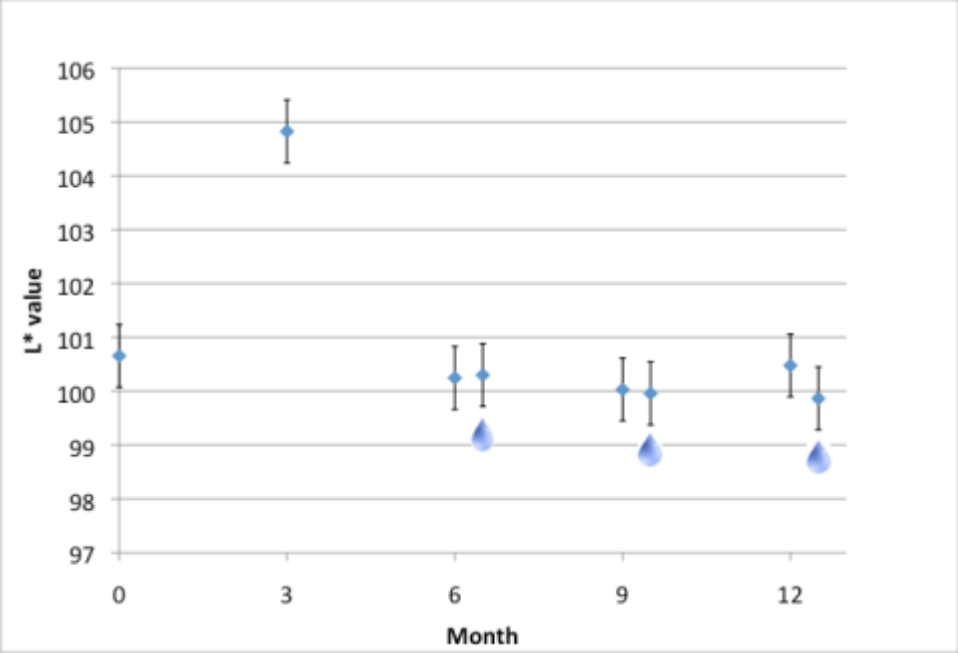

(a)

Figure 4.21: Average L* Readings for Lab Keim (a) Barrier Specimen and (b) Slab Specimen

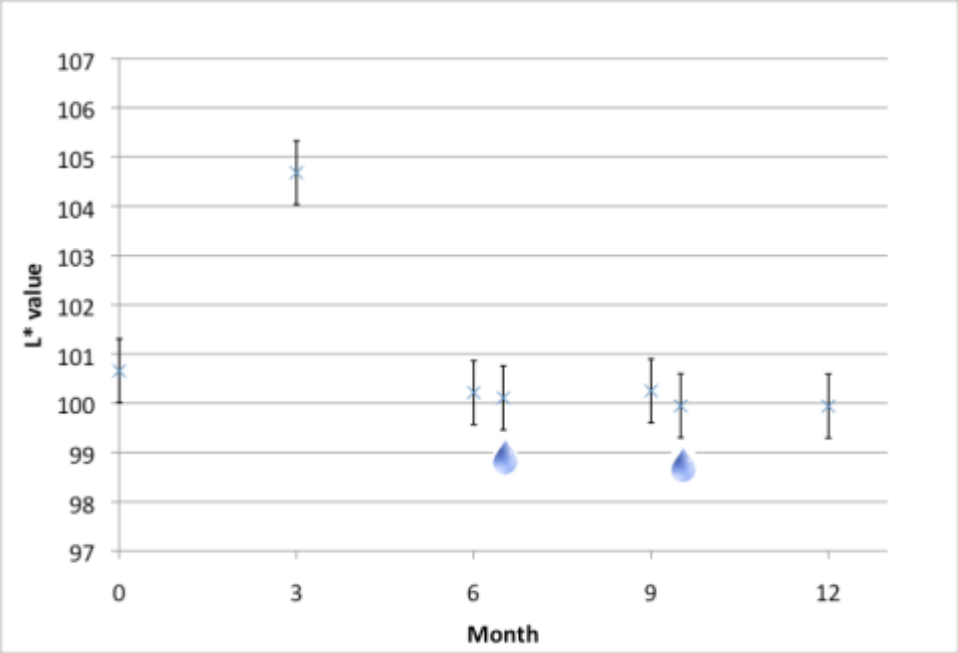

(b)

Figure 4.21, continued

The Keim-coated specimens at the Lab site saw slight reductions in average L* readings over one-year outdoor exposure. In both the case of the barrier and slab specimen, this decrease was within the margin of error of the initial reading.

The TxActive coating maintained its brightness more efficiently than the Keim coating and maintained or increased in brightness regardless of the field site or type of specimen. The Keim coating reduced significantly in brightness over one year exposure in all Houston and Austin specimens and slightly for the Lab specimens. Based on these results, it is likely that photocatalytic efficiency was reduced after outdoor exposure more for the Keim coating than for the TxActive coating. All data can be verified by the photographs taken during each site visit, which are located in Appendix B.

4.3.3 Temperature

The temperature of each specimen was measured using an infrared thermometer for the duration of the outdoor exposure period. This information was used to verify the temperatures used in the environmental chambers were appropriate. The data for temperature are not available for the 0 and 3 month intervals for Houston or the 0 interval for the Austin or Lab sites. The results are presented in Appendix B.

Chapter 5: Conclusions and Future Work

5.1 CONCLUSIONS

The goal of this project was to evaluate several commercial photocatalytic coatings used in the removal of pollution near highways. Durability and pollution removal of each coating were measured through several tests. Durability was evaluated through x-ray diffraction and scanning electron microscopy before and after exposure, while pollution removal was measured through ion chromatography on wash water samples. Efficiency of sunlight penetration to the outdoor samples was also evaluated by measuring brightness of each coating. All of the tests were conducted at three-month intervals throughout one year outdoor exposure for three field sites.

Several conclusions can be drawn from this study. A few of the more important deductions that can be made are as follows:

- Paint and spray coating applications are significantly easier to apply than stucco; therefore, cost of application for large-scale projects is an important consideration when selecting an appropriate photocatalytic coating for the removal of highway-generated pollutants.
- Phase of titanium dioxide contained in the photocatalytic coating plays an important role in its pollution removal capacity. Anatase seems to have stronger photocatalytic removal capability than rutile.
- XRD patterns remained stable over one-year outdoor exposure for all coatings. Photocatalytic material was present in the Keim and TxActive samples before and after the exposure period. No photocatalytic material was found in the XRD pattern either before or after exposure for the Pureti specimen.

- Based on SEM images, the distribution of titanium on the coated surface and cross section samples remained constant for the TxActive and Keim specimens. The distribution of titanium appeared to decrease for Pureti. This may indicate that the Pureti coating is not durable for outdoor exposure near highway locations.
- Water washes may not be an efficient way of determining photocatalytic pollutant removal outdoors based on low concentrations of nitrates and nitrites seen in this project. However, TxActive specimens did have the highest readings of those that were observed, which could indicate higher pollutant removal in the field for this coating.
- Brightness was maintained or increased for all TxActive-coated specimens after one-year outdoor exposure for all three field sites. This indicates that surface contaminants are either not adhering to this coating or being washed off efficiently. Thus, exposure of the coating to the sunlight necessary to activate photocatalytic process is occurring.
- Brightness decreased for all Keim-coated specimens after one-year outdoor exposure for all three field sites. The decrease was more substantial for the Houston and Austin field sites, where surface contaminants were more likely to adhere to the surface due to the proximity and volume of nearby highway traffic, than for the Lab site. This could indicate that photocatalytic activity decreases during exposure for Keim-coated specimens that are placed outdoors.

5.2 RECOMMENDATIONS

At the conclusion of this project, several recommendations can be made to continue to understand durability and photocatalytic efficiency of commercial coatings in areas of Texas with high volumes of traffic:

- Evaluate the effect of the type of aggregate on photocatalytic removal to understand whether the use of siliceous aggregate might diminish or increase photocatalytic efficiency.
- More long-term testing is recommended to determine whether coatings are stable under outdoor conditions after 2 or more years.
- Evaluate the accuracy of ion chromatography tests to determine whether higher levels of nitrates and nitrites can be achieved with longer intervals between rainfall, closer proximity of specimens to source of pollution, or another means.
- Conduct testing to correlate the decrease of brightness on the CIE scale to UV penetration and photocatalytic removal to determine whether decrease in brightness has a direct correlation with reduced pollutant removal.
- Direct measurement of air pollution in outdoor exposure locations is recommended to gain the best understanding of pollution removal capability at real-world scale.
- Further durability testing including impact testing and long-term stability of coatings to verify suggested coating lifetimes issued by manufacturers.

Appendix A: Concrete Mixture Information

A.1 TRICON PRECAST CONCRETE BARRIER MIXTURE DESIGN SHEET

AGGREGATE CHARACTERISTICS						Revised Date	00/20/09
Aggregate	**SP Gravity**	**SSD Unit Wt LBS / Cu. Ft.**	**% Solids**	**Source**			**F.M./Grade**
Fine [FA]	2.62	106.90	65.49%	Hanson Servtex			3.05
Coarse [CA]	2.59	96.30	59.68%	Hanson Servtex			4

DESIGN FACTORS							
			w/cm Ratio	**0.34**	**CA% of Total Agg. by Vol.**	**50.92%**	
CA Factor [CAF]	0.650		**Air Factor [AF]**	2.0%	**Theor. Unit Wt of Conc.**	**150.33**	
Cement Factor [CF]	6.00	sks/cy	**Cement Source / Type**	Capitol Cement Type III			
Water Factor [WF]	3.75	gal/sk	**Water Source**	Garden Ridge Municipal Water			
SCM 1 Percent	25.0%		**SCM 1 Source/Type**	Headwaters - Limestone Class F	**SP.GR.**	2.36	
SCM 2 Percent			**SCM 2 Source/Type**		**SP.GR.**		

Batch Design [One Sack]	Volume: 1-Sk Batch [Cu Ft]		Vol to Wt [Lb] Vol x 62.5 x Sp Gr	1-Sack Batch Wt	Full Size Batch Factor	Wts
1. Concrete Yield = CuFt per CuYd / CF	27 / 6.0	4.500				
2. Volume CA = Yield x CAF x Solids	4.500 x 0.65 x 0.597	**1.727**	x 62.4 x 2.59	279.11	6.00	* **1,675**
3. Volume Mortar = Yield - Vol CA	4.500 - 1.727	2.773				
4. Volume Water = WF / Gals Wat per CuFt	3.8 / 7.5	**0.500**	x 62.4 x 1.00	31.20	6.00	* **187**
5. Volume SCM 1	94 / 62.4 x 25% / 2.36	**0.160**	x 62.4 x 2.36	23.50	6.00	**141**
6. Volume SCM 2	94 / 62.4 x 0% / 0.00	**0.000**	x 62.4 x 0	0.00	6.00	**-**
7. Volume One Sk Cement	94 / 62.4 x 75% / 3.15	**0.359**	x 62.4 x 3.10	69.44	6.00	**423**
8. Volume Entrained Air = Yield x AF	4.500 x 0.020	**0.090**				
9. Volume Paste = Vol Cem+Water+Air	0.518 + 0.500 + 0.090	1.108				
10. Volume FA = Vol Mortar - Paste	2.773 - 1.108	**1.665**	x 62.4 x 2.62	271.10	6.00	* **1,627**
11. Yield [Summation of 2, 4, 5, 6, 7, 8, & 10 to Check Number 1 above]		**4.501**		TOTAL Batch Wts		* **4,053**
12. FA Factor = Vol FA / FA Solids x Vol Mortar =	1.665 / 0.655 x 2.773	= 1.665 / 1.816	= 0.92	* Correct for Free Moisture & Absorption		

A.2 TRICON PRECAST CONCRETE BARRIER MIXTURE CYLINDER STRENGTH RESULTS & ADMIXTURE INFORMATION

Cyl No	Age	Area	Load	Stress
1	19 Hours	12.50	65,680	5,250
2	19 Hours	12.50	64,540	5,160
			19 Hours Hr Avg	**5,210**

Cyl No	Age	Area	Load	Stress
3	3 day	12.50	79,410	6,350
4	3 day	12.50	82,700	6,620
			3 Day Avg	**6,490**

Cyl No	Age	Area	Load	Stress
5	7 day	12.50	92,220	7,380
6	7 day	12.50	90,290	7,220
			7 Day Avg	**7,300**

Cyl No	Age	Area	Load	Stress
7	14 day	12.50	101,640	8,130
8	14 day	12.50	99,260	7,940
			14 Day Avg	**8,040**

Cyl No	Age	Area	Load	Stress
9	28 day	12.50	104,310	8,340
10	28 day	12.50	105,630	8,450
			28 Day Avg	**8,400**

Remarks	
Entrained Air Content	2.9
Initial Set (hrs)	n/a

Slump	6.50	Admixture	Type	Sika 2110	Dosage (oz/100 lbs)	7	% solids	40
Air Temperature	89	Admixture	Type	Plastiment	Dosage (oz/100 lbs)	2	% solids	33
Concrete Temperature	89	Admixture	Type		Dosage (oz/100 lbs)		% solids	
Actual Unit Weight	148.80	Admixture	Type		Dosage (oz/100 lbs)		% solids	

A.3 Mixture Design Used In The Laboratory-Mixed Slab Specimens

MATERIALS PROPERTIES

Material	BSG* (SSD)	AC** (OD)	Description
Cement	3.1	NA	
Fly Ash	2.36		
Other:			
Water	1	NA	
Rock	2.59	1.84	
Sand	2.61	1.8	

* BSG = Bulk Specific Gravity
** AC = Absorption Capacity

THEORETICAL MIX PROPORTIONS PER CU. YD.

Material	Weight, lb.	Volume, cu. ft.	Dosage, fluid ounces
Cement	423	2.18672457	
Fly Ash	141	0.95746415	
Other:			
Water	187	2.99679487	
Rock (SSD)	1675	10.3640729	
Sand (SSD)	1627	9.98993025	
Air	2.00%	0.54	
		27.03	
Admixtures:			
Sika 2110			7.0
Plastiment			2.0

BATCHING INFORMATION

Batch Size = 2.577372129 cu.ft.

Appendix B: Field Site Data

B.1: Photographs of Specimens During Site Visits

B.1: Houston Control Barrier Specimen Photographs Throughout Exposure

Initial

6 months

9 months

12 months

B.2: Houston TxActive Barrier Specimen Photographs Throughout Exposure

Initial

6 months

9 months

12 months

B.3: Houston Keim Barrier Specimen Photographs Throughout Exposure

Initial

6 months

9 months

12 months

B.4: Houston Pureti Barrier Specimen Photographs Throughout Exposure

Initial

6 months

9 months

12 months

B.5: Houston Control Slab Specimen Photographs Throughout Exposure

Initial

6 months

9 months

12 months

B.6: Houston TxActive Slab Specimen Photographs Throughout Exposure

Initial

6 months

9 months

12 months

B.7: Houston Keim Slab Specimen Photographs Throughout Exposure

Initial

6 months

9 months

12 months

B.8: Houston Pureti Slab Specimen Photographs Throughout Exposure

Initial

6 months

9 months

12 months

B.9: Austin Control Barrier Specimen Photographs Throughout Exposure

Initial

6 months

9 months

12 months

B.10: Austin TxActive Barrier Specimen Photographs Throughout Exposure

Initial

6 months

9 months

12 months

B.11: Austin Keim Barrier Specimen Photographs Throughout Exposure

Initial

6 months

9 months

12 months

B.12: Austin Pureti Barrier Specimen Photographs Throughout Exposure

Initial

6 months

9 months

12 months

B.13: Austin Control Slab Specimen Photographs Throughout Exposure

Initial

6 months

9 months

12 months

B.14: Austin TxActive Slab Specimen Photographs Throughout Exposure

Initial

6 months

9 months

12 months

B.15: Austin Keim Slab Specimen Photographs Throughout Exposure

Initial

6 months

9 months

12 months

B.16: Austin Pureti Slab Specimen Photographs Throughout Exposure

Initial

6 months

9 months

12 months

B.17: Lab Control Barrier Specimen Photographs Throughout Exposure

Initial

6 months

9 months

12 months

B.18: Lab TxActive Barrier Specimen Photographs Throughout Exposure

Initial

6 months

9 months

12 months

B.19: Lab Keim Barrier Specimen Photographs Throughout Exposure

Initial

6 months

9 months

12 months

B.20: Lab Pureti Barrier Specimen Photographs Throughout Exposure

Initial

6 months

9 months

12 months

B.21: Lab Control Slab Specimen Photographs Throughout Exposure

Initial

6 months

9 months

12 months

B.22: Lab TxActive Slab Specimen Photographs Throughout Exposure

Initial

6 months

9 months

12 months

B.23: Lab Keim Slab Specimen Photographs Throughout Exposure

Initial

6 months

9 months

12 months

B.24: Lab Pureti Slab Specimen Photographs Throughout Exposure

B.2 Temperature Data for All Site Visits

Table B.1: Temperature Data for Houston Site

	3 Months				6 Months				9 Months				12 Months			
Date	8/16/11				11/17/11				1/30/12				4/4/12			
Time	10:30 AM				9:30 AM				9:30 AM				9:30 AM			
Weather	Sunny and hot with sparse clouds				Sunny				Sparse clouds							
	PURETi	TxActive	Control	KEIM	PURETi	TxActive	Control	KEIM	PURETi	TxActive	Control	KEIM	PURETi	TxActive	Control	KEIM
Temp: Barrier (°F)	Unavailable				75	63	74.5	60.8	70.2	62.6	69.1	63.8	73.3	71.8	73.2	71.9
Temp: Slab (°F)					63.1	49.9	61.3	49.9	69.1	62.7	69.4	63	72.1	70.9	69.8	70.4

Table B.2: Temperature Data for Austin Site

	3 Months				6 Months				9 Months				12 Months			
Date	8/30/11				12/1/11				2/9/12				3/23/12			
Time	9:15 AM				2:30 PM				9:30 AM				1:00 PM			
Weather	Sunny and hot				Sunny, few clouds				Sunny, few clouds				sunny and hot			
	PURETi	TxActive	Control	KEIM	PURETi	TxActive	Control	KEIM	PURETi	TxActive	Control	KEIM	PURETi	TxActive	Control	KEIM
Temp: Barrier (°F)	74.9	76.5	77.3	76.7	68.5	66.2	67.3	65.7	45.5	42.8	44.6	41.7	57	53	57	50
Temp: Slab (°F)	63.3	62.2	64.4	63.9	75.6	70.2	77.4	68	55.6	50.7	56.8	48.1	86	70	90	65

Table B.3: Temperature Data for Lab Site

	3 Months				6 Months				9 Months				12 Months			
Date	9/1/11				12/10/11				2/8/12				3/22/12			
Time	9:00 AM				9:00 AM				12:30 PM				1:00 PM			
Weather	Sunny and hot				overcast				Partly cloudy				sunny and clear			
	PURETi	TxActive	Control	KEIM	PURETi	TxActive	Control	KEIM	PURETi	TxActive	Control	KEIM	PURETi	TxActive	Control	KEIM
Temp: Barrier (°F)	93.6	84.2	101.7	84.4	45.2	45.2	45.7	45	63	55.1	71.4	55	83.7	74.5	84.7	74.8
Temp: Slab (°F)	100.2	90.3	101.2	89.6	45.6	45.6	46.6	44.8	64.1	55.8	71.9	56.1	95.5	83.7	101.4	84

References

Agrios, A., & Pichat, P. (2005). State of the art and perspectives on materials and applications of photocatalysis over TiO2. *Journal of Applied Electrochemistry , 58* (35), 665-663.

ASTM C 138. (2007). Standard Test Method for Density (Unit Weight), Yield, and Air Content (Gravimetric) of Concrete. West Consohocken, PA: American Society of Testing and Materials.

ASTM C127. (2007). Standard Test for Density, Relative Density (Specific Gravity), and Absorption of Coarse Aggregate. West Consohocken, PA: American Society of Testing and Materials.

ASTM C128. (2007). Standard Test Method for Density, Relative Density (Specific Gravity), and Absorption of Fine Aggregate. West Consohocken, PA: American Society of Testing and Materials.

ASTM C143. (2010). Standard Test Method for Slump of Hydraulic-Cement Concrete. West Consohocken, PA: American Society of Testing and Materials.

ASTM C150. (2011). Standard Specification for Portland Cement. West Consohocken, PA: American Society of Testing and Materials.

ASTM C192. (2007). Standard Practice for Making and Curing Concrete Specimens in the Laboratory. West Consohocken, PA: American Society of Testing and Materials.

ASTM C231. (2010). Standard Test Method for Air Content of Freshly Mixed Concrete by the Pressure Method. West Consohocken, PA: American Society of Testing and Materials.

ASTM C39. (2010). Standard Test Method for Compressive Strength of Cylindrical Concrete Specimens. West Consohocken, PA: American Society of Testing and Materials.

ASTM C618. (2008). Standard Specification for Coal Fly Ash and Raw or Calcined Natural Pozzolan for Use in Concrete. West Consohocken, PA: American Society of Testing and Materials.

ASTM C897. (2005). Standard Specification for Aggregate for Job-Mixed Portland Cement-Based Plasters. West Consohocken, PA: American Society of Testing and Materials.

ASTM C926. (2011). Standard Specification for Application of Portland Cement Plaster. West Consohocken, PA: American Society of Testing and Materials.

Auvinen, J., & Wirtanen, L. (2008). The influence of photocatalytic interior paints on indoor air quality. *Atmospheric Environment , 42*, 4101-4112.

Beeldens, A., & Van Gemert, D. (2004). Experimental investigation of Efficiency of TiO2-cement coating for self-cleaning and air purification. *RILEM International Symposium on Environment-Conscious Materials and Systems for Sustainable Development* (pp. 353-359). Koriyama: RILEM.

Bygott, C., Maltby, J., Stratton, J., & McIntyre, R. (2007). Photocatalytic Coatings for the Construction Industry. *International RILEM Symposium on Photocatalysis, Environment, and Construction Materials* (pp. 251-258). Florence: RILEM.

Cassar, L. (2004). Photocatalysis of Cementitous Materials: Clean Buildings and Clean Air. *MRS Bulletin , 29*, 328-331.

Chen, J., & Poon, C. (2009). Photocatalytic Cementitious Materials: Influence of the Microstructure of Cement Paste on Photocatalytic Pollution Degredation. *Environ. Sci. Technol. , 43*, 8948-8952.

Chen, J., Kou, S., & Poon, C. (2011). Photocatalytic cement-based materials: Comparison of nitrogen oxides and toluene removal potentials and evaluation of self-cleaning performance. *Building and Environment , 46*, 1827-1833.

Ctibor, P., Stengl, V., Zahalka, F., & Murafa, N. (2010). Microstructure and performance of titanium oxide coatings sprayed by oxygen-acetylene flame. *Photochemical & Photobiological Sciences , 10*, 403-407.

Dehn, F., Bahnemann, D., & Bilger, B. (2004). Development of Photocatalytically Active Coatings for Concrete Substrates. *RILEM International Symposium on Environment-Conscious Materials and Systems for Sustainable Development* (pp. 347-352). Koriyama: RILEM.

Diamanti, M., Ormellese, M., & Pedeferri, M. (2008). Characterization of photocatalytic and superhydrophillic properties of mortars containing titanium dioxide. *Cement and Concrete Research , 38*, 1349-1353.

Drimalas, T. (2007). *Laboratory and Field Evaluations of External Sulfate Attack.* The University of Texas at Austin, Civil Engineering. Austin: UT Austin.

Dylla, H., Hassan, M. M., Mohammad, L. N., Rupnow, T., & Wright, E. (2010). Evaluation of Environmental Effectiveness of Tianium Dioxide Photocatalyst Coating for Concrete Pavement. *Transportation Research Record: Journal of the Transportation Research Board , 2164*, 46-51.

Essroc. (2010). *TxActive Project Profiles*. Retrieved 2010 йил 11-11 from Essroc TxActive Photocatalytic Cements: http://www.txactive.us/project.html

Fernandez, A., Lassaletta, G., Jimenez, V. M., Justo, A., Gonzalez-Elipe, A. R., Herrmann, J.-M., et al. (1995). Preparation and characterization of TiO2 photocatalysts supported on various rigid supports (glass, quartz, stainless steel). Comparitive studies of photocatalytic activity in water purification. *Applied Catalysis B: Environmental , 7*, 49-63.

Folli, A., Pochard, I., Nonat, A., Jakobsen, U., Shepherd, A. M., & Macphee, D. E. (2010). Engineering Photocatalytic Cements: Understanding TiO2 Surface chemistry to control and modulate Photocatalytic Performances. *J. Am. Ceram. Soc. , 93*, 3360-3369.

Fujishima, A., Zhang, X., & Tryk, D. A. (2008). TiO2 photocatalysis and related surface phenomena. *Surface Science Reports , 63*, 515-582.

Guerrini, G., Plassais, A., Pepe, C., & Cassar, L. (2007). Use of Photocatalytic Cementitious Materials for Self-Cleaning Applications. *International RILEM Symposium on Photocatalysis, Environment, and Construction Materials* (pp. 219-226). Florence: RILEM.

Hassan, M., Dylla, H., Mohammad, L. N., & Rupnow, T. (2010). Evaluation of titanium dioxide photocatalyst coating for concrete pavement. *Construction and Building Materials , 24*, 1456-1461.

Husken, G., Hunger, M., & Brouwers, H. (2007). Comparative Study on Cementitious Products Containing Titanium Dioxide as Photo-Catalyst. *Proceedings of International RILEM Syposium on Photocatalysis, Environment, and Construction Materials* (pp. 147-154). Florence: RILEM.

Husken, G., Hunger, M., & Brouwers, H. (2009). Experimental study of photocatalytic concrete products for air purification. *Building and Environment , 44*, 2463-2474.

Jayapalan, A., Lee, B. Y., Fredrich, S. M., & Kurtis, K. E. (2010). Influence of Additions of Anatase TiO2 Nanoparticles on Early-Age Properties of Cement-Based Materials. *Transportation Research Record: Journal of hte Transportation Research Board , 2141*, 41-46.

Kawakami, M., Furumura, T., & Tokushige, H. (2007). NOx Removal Effects and Physical Properties of Cement Mortar Incorporating Titanium Dioxide Powder. *Proceedings of International RILEM Symposium on Photocatalysis, Environment, and Construction Materials* (pp. 163-170). Florence: RILEM.

Lackhoff, M., Prieto, X., Nikolaus, N., Dehn, F., & Reinhard, N. (2003). Photocatalytic activity of semiconductor-modified cement-influence of semiconductor type and cement ageing. *Applied Catalysis B: Environmental , 43*, 205-216.

Laufs, S., Burgeth, G., Duttlinger, W., Kurtenbach, R., Maban, M., Thomas, C., et al. (2010). Conversion of nitrogen oxides on commercial photocatalytic dispersion paints. *Atmospheric Environment , 44*, 2341-2349.

Lee, B., Thomas, J., Treager, M., & Kurtis, K. E. (2010). Influence of TiO2 Nanoparticles on Early C3S Hydration. *Journal of the American Ceramic Society , 93*, 3399-3405.

Motohashi, K., & Inukai, T. (2007). Self-Cleaning Performance Evaluation of Commercial Photocatalyst Coating Materials Through 5 Years Outdoor Exposure. *Proceedings of International RILEM Symposium on Photocatalysis* (pp. 307-313). Florence: RILEM.

Motohashi, K., Inukai, T., & Konishi, T. (2004). Performance Evaluation of Self-Cleaning Effect for Photocatalyst-Applied Exterior Finishing Materials Throguh Outdoor Exposure Test and Laboratory Test. *RILEM International Symposium on Environment-Conscious Materials and Systems for Sustainable Development* (pp. 27-34). Koriyama: RILEM.

Nord, A., Syardh, A., & Tronner, K. (1994). Air Pollution Levels Reflected in Deposits on Building Stone. *Atmospheric Environment , 28*, 2615-2622.

Ozawa, T., Iwasaki, M., Tada, H., Akita, T., Tanaka, K., & Ito, S. (2005). Low-temperature synthesis of anatase-brookite composite nanocrystals: the junction effect on photocatalytic activity. *Journal of Colloid and Interface Science , 281*, 510-513.

Pachego-Torgal, F., & Jalali, S. (2011). Nanotechnology: Advantages and drawbacks in the field of construction and building materials. *Construction and building materials , 25*, 582-590.

Pepe, C., Amadelli, R., Pimpinelli, N., & Cassar, L. (2004). Doped-TiO2/Cement matrices Photoactive Materials. *RILEM International Symposium on Environment-Conscious Materials and Systems for Sustainable Development* (pp. 331-336). Koriyama: RILEM.

Pesek, P. (2011). *Temperature, Stress, and Strength Development of Early-Age Bridge Deck Concrete.* The University of Texas at Austin, Civil Engineering. Austin: UT Austin.

Poon, C., & Cheung, E. (2007). NO removal efficiency of photocatalytic paving blocks prepared with recycled materials. *Construction and Building Materials , 21*, 1746-1753.

Potenza, G., Licciulli, A., Diso, D., Franza, S., Calia, A., Lettieri, M., et al. (2007). Surface Engineering on Natural stone Through TiO2 Photocatalytic Coatings. *Proceedings of International RILEM Symposium on Photocatalysis, Environment, and Construction Materials* (pp. 315-322). Florence: RILEM.

Rachel, A., Subrahmanyam, M., & Boule, P. (2002). Comparison of photocatalytic efficiencies of TiO2 in suspended and immobilized form for the photocatalytic degredation of nitrobenzenesulfonic acids. *Applied Catalysis B: Environmental , 37*, 301-308.

Ramirez, A., Demeestere, K., De Belie, N., Mantyla, T., & Levanen, E. (2010). Titanium dioxide coated cementitious materials for air purifying purposes: Preparation, characterization, and toluene removal potential. *Building and Environment , 45*, 832-838.

Ruot, B., Plassais, A., Olive, F., Guillot, L., & Bonafous, L. (2009). TiO2-containing cement pastes and mortars: Measurements of the photocatalytic efficiency using a rhodamine-B based colourimteric test. *Solar Energy , 83*, 1794-1801.

Shimohigoshi, M., & Saeki, Y. (2007). Research and Applications of Photocatalyst Tiles. *Proceedings of International RILEM Symposium on Photocatalysts, Environment, and Construction Materials* (pp. 291-297). Florence: RILEM.

Simms, G. (2010). Dalton State University Tower. (A. Terpeluk, Interviewer)

Stone, W. (2010). Missouri DOT Project. (A. Terpeluk, Interviewer)

Strini, A., Cassese, S., & Schiavi, L. (2005). Measurement of benzene, toluene, ethylbenzene, and o-xylene gas phase photodegredation by titanium dioxide dispersed in cementitious materials using a mixed-flow reactior. *Applied Catalysis B: Environmental , 61*, 90-97.

Toma, F., Bertrand, G., Klein, D., & Coddet, C. (2004). Photocatalytic removal of nitrogen oxides via titanium dioxide. *Environ. Chem. Lett. , 2*, 117-121.

Vallee, F., Ruot, B., Bonafus, L., Guillot, L., Pimpinelli, N., Cassar, L., et al. (2004). Cementitious Materials for Self-Cleaning and Depolluting Surfaces. *RILEM International Symposium on Environment-Conscious Materials and Systems for Sustainable Development* (pp. 337-346). Koriyama: RILEM.

Williams, S. (2005). *Structures Affected by Premature Concrete Deterioration: Diagnosis and Assessment of Deterioration Mechanisms.* University of Texas at Austin, Civil Engineering. Austin: UT Austin.

World Health Organization. (2011 йил 1-September). *Media centre: Air quality and health fact sheet*. Retrieved 2012 йил 13-January from World Health Organization: www.who.int/mediacentre/factsheets/fs313/en/index.html

Yu, J. (2003). *Deactivation and Regeneration of Environmentally Exposed Titanium Dioxide Based Products.* Environmental Protection Department, HKSAR. Hong Kong: The Chinese University of Hong Kong.

Zhang, M., & Li, H. (2011). Pore structure and chloride permeability of concrete containing nano-particles for pavement. *Construction and Building Materials , 25*, 608-616.

Znaidi, L., Seraphimova, R., Bocquet, J. F., Colbeau-Justin, C., & Pommer, C. (2001). A semi-continuous process for the synthesis of nanosize TiO2 powders and their use as photocatalysts. *Materials Research Bulletin , 36*, 811-825.